To appear in ***Handbook of Experimental Fluid Dynamics***, Chapter 5.4,
editors: J. Foss, C. Tropea and A. Yarin, Springer-Verlag (2007).

Molecular Tagging Velocimetry

Manoochehr M. Koochesfahani[1] and Daniel G. Nocera[2]

[1]Department of Mechanical Engineering
Michigan State University, East Lansing, MI 48824

[2]Department of Chemistry, 6-335
Massachusetts Institute of Technology, Cambridge, MA 02139

1. Introduction

Molecular Tagging Velocimetry (MTV) is a whole field optical technique that relies on molecules that can be turned into long lifetime tracers upon excitation by photons of appropriate wavelength. These molecules are either premixed or naturally present in the flowing medium (i.e. unseeded applications). Typically a pulsed laser is used to "tag" the regions of interest, and those tagged regions are interrogated at two successive times within the lifetime of the tracer. The measured Lagrangian displacement vector provides the estimate of the velocity vector. This technique can be thought of as essentially a *molecular* counterpart of Particle Image Velocimetry (PIV), and it can offer advantages compared to particle-based techniques where the use of seed particles is not desirable, difficult, or may lead to complications. Figure 1 illustrates one implementation of the technique where the particular tracer used is a water-soluble phosphorescent supramolecule. A planar grid of intersecting laser beams, formed from a pulsed excimer laser (20 ns pulse width, 308 nm wavelength), turns on the luminescence of the supramolecules that are premixed in a water flow of a vortex ring approaching a solid wall at normal incidence (Gendrich et al. 1997). The displacement of the tagged regions is determined, in this case, using a direct spatial correlation method. The conventional planar imaging shown in Figure 1 provides information on two components of the velocity vector, the projection onto the viewed plane. Stereo imaging can produce the complete three components of the velocity vector (Bohl et al. 2001).

While the earliest use of MTV can be traced back at least three decades, this technique has seen significant advances over the past fifteen years (sometimes under alternate titles such as laser-induced photochemical anemometry, LIPA, and flow tagging velocimetry). The ability to non-intrusively tag the molecules in a flowing medium and observe their subsequent evolution offers other possibilities besides only velocimetry in fluid flows. Depending on tracer properties and the method of implementation, molecular tagging can be used for flow visualization, simultaneous quantification of velocity and scalar (concentration or temperature)

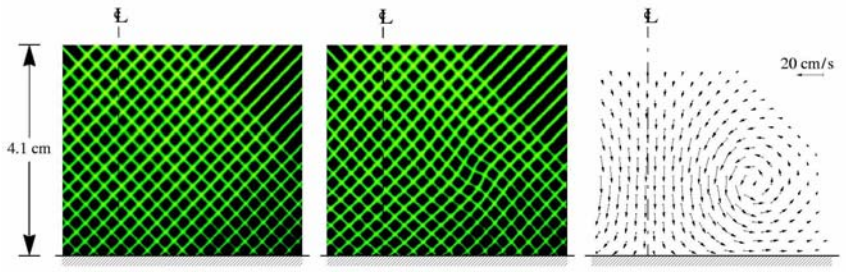

Fig. 1. Typical MTV image pairs and the resultant velocity field (Gendrich et al. 1997). The flow shown is from a vortex ring impacting on a flat wall at normal incidence. The axis of symmetry is indicated by the dashed lines. (a) The grid imaged 1 μs after the laser pulse. (b) The same grid imaged 8 ms later. (c) The velocity field derived from (a) and (b).

fields, and novel methods in studying the Lagrangian evolution of scalar fields, entrainment and mixing. As we describe the various elements involved in using molecular tagging techniques, and in particular molecular tagging velocimetry, we draw attention to several review articles which have appeared in the past (Falco & Nocera 1993; Koochesfahani et al. 1996; Koochesfahani 1999; Lempert & Harris 2000a), in addition to a special issue of *Measurement Science and Technology* on this topic (Koochesfahani 2000).

2. The Photochemistry of MTV: Molecular Tracers and Chemical Mechanisms

A molecular complex is suitable for molecular tagging applications if its lifetime as a tracer is long enough relative to the flow convection time scale to allow sufficient displacement of the tagged regions during the interrogation time. The photophysical properties of the tracer, in turn, dictate the wavelength and number of photon sources needed for creating the tracer (i.e. the tagging process) and those needed for interrogation.

All MTV techniques are based on the chemistry of molecules in electronic excited states. Normally residing in dark or ground states, molecules enter excited states when they absorb energy from the environment. Electronically excited molecules are generally very reactive, eventually returning either to their original ground state or to a new ground state molecule. The departure of a molecule from its excited state may occur in the absence of a reacting partner (called an intramolecular decay process) or with the help of a second molecule (called an intermolecular decay process), as shown schematically in Figure 2.

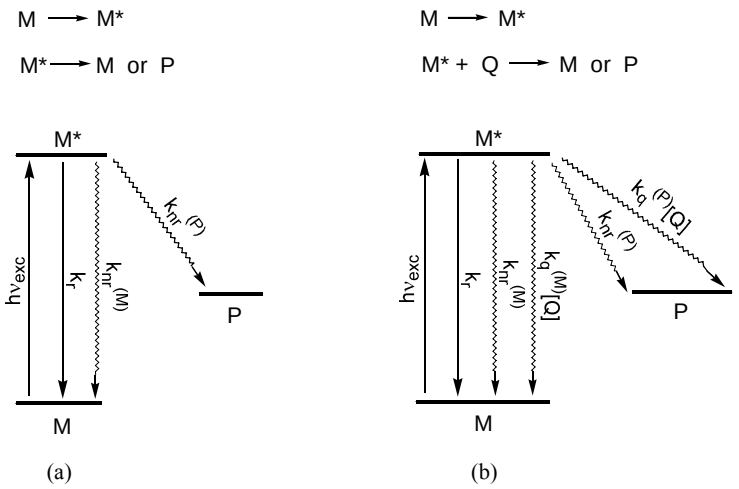

Fig. 2. (a) Simple excited state diagram for intramolecular decay processes of a molecule in an excited state, M^*. The radiative rate constant k_r and nonradiative rate constant $k_{nr}^{(M)}$ describe the conversion of M^* to its ground state M by photon and thermal emission, respectively. $k_{nr}^{(P)}$ is the rate constant describing the return of M^* to a new molecule P. (b) The excited state diagram including intramolecular and intermolecular decay processes of a molecule in an excited state, M^*. The quenching rate constants $k_q^{(M)}$ and $k_q^{(P)}$ describe the intermolecular conversion of M^* by quencher Q to its ground state M or new ground state molecule P.

Figure 2(a) depicts the intramolecular processes that govern the decay of an isolated excited state molecule to its ground state. Competing photon emission (radiative) and thermal (nonradiative) relaxation pathways are described by the radiative (k_r) and nonradiative (k_{nr}) rate constants, respectively. The radiative rate constant is an intrinsic property of the molecule and it reflects the probability of the excited state emitting a photon of a given frequency; k_r is directly related to the ability of the molecule to absorb light, described by the oscillator strength or the molar absorptivity constant (Balzani and Carassiti 1970; Forster 1975; Wayne 1988). k_{nr} encompasses all decay pathways that do not lead to photon emission. Nonradiative decay most typically entails the conversion of an excited state's electronic energy into high-energy vibrations of the ground state molecule (Jortner et al. 1969; Freed 1978; Lin 1980). Vibrational relaxation to the equilibrated ground state molecule (M) is accompanied by the concomitant release of heat ($k_{nr}^{(M)}$); alternatively, the excess vibrational energy may be manifested in the creation of a different ground state molecule ($k_{nr}^{(P)}$), called the photoproduct. The overall nonradiative decay rate constant, k_{nr}, is simply $k_{nr} = k_{nr}^{(M)} + k_{nr}^{(P)}$.

The interplay between k_r and k_{nr} determines the fundamental properties of molecules in excited states (Balzani and Carassiti 1970; Turro 1978). The intensity of luminescence, I_o, is directly dependent on the luminescence efficiency, usually called the emission quantum yield, Φ_e, which is the ratio of the number of pho-

tons emitted per photons absorbed. The emission quantum yield is directly related to k_r and k_{nr} by the following expression

$$I_o \sim \Phi_e = \frac{k_r}{k_r + k_{nr}} = k_r \tau_o, \qquad (1)$$

where τ_o is the observed lifetime of the electronic excited state,

$$\tau_o = \frac{1}{k_r + k_{nr}} \quad . \qquad (2)$$

Nonradiative relaxation pathways usually dominate (i.e. $k_{nr} >> k_r$) and, as can be seen from Eq. (1), molecules under this condition will remain dark upon excitation. However, when thermal emission is inefficient with regard to photon emission (i.e. $k_r >> k_{nr}$), excited states will literally light up or luminesce.

Two types of luminescence are of significance to MTV techniques: fluorescence and phosphorescence. In the ground state, virtually all molecules reside in electronic states in which the electrons are paired. For this situation, a molecule is said to be in a singlet ground state. Quantum mechanical rules dictate that the most probable transitions to excited states will be to other singlet excited states. Fluorescence is the radiative process that accompanies the relaxation of a molecule from a singlet excited state to its singlet ground state. Because singlet-to-singlet transitions are quantum mechanically allowed, they occur with a high probability. Hence k_r is large, ranging from 10^8 to 10^{10} s^{-1}. From the perspective of Equations (1) and (2), there are two consequences of such large values of k_r. Nonradiative decay channels k_{nr} are generally not competitive with k_r (i.e. $k_r >> k_{nr}$). As deduced directly from Equation 1, the emission intensity of a fluorescent excited state is therefore intense. Moreover, the lifetime of a fluorescent excited state will also approach that of k_r^{-1} (see Eq. 2); thus fluorescent lifetimes are short, on the order of 1-100 nanoseconds (ns) with most fluorescent lifetimes ~ 2-10 ns.

Conversely, phosphorescence is long-lived because the transitions between the excited state and ground state are forbidden. In a phosphorescent excited state, the electrons are triplet-paired or aligned with each other. Here the absorption process occurs between the singlet ground state and an excited state of different spin. Quantum mechanically, this is a forbidden transition, and hence k_r is small. The radiative decay rates can therefore approach seconds and the phosphorescence lifetimes can be large (owing to the small k_r). However, the phosphorescence intensity from the spin forbidden excited state may be significantly weaker than fluorescence because k_{nr} will become competitive with k_r on the micro- to millisecond time scale. Moreover, because the absorption cross-section of the triplet state is small, it is usually not produced by direct absorption. Alternatively, the triplet excited state is usually populated from a correspondent singlet state by the intersystem crossing (isc) process. Because the triplet is of less energy than the singlet, the wavelength for phosphorescence is significantly red-shifted from the absorption profile. Thus, whereas the wavelength difference between the absorption and emission profile (known as the Stokes shift) may be relatively small for fluorescence, a large shift between the wavelengths of absorption and phosphorescence is typically observed.

Equations (1) and (2) only consider the intramolecular decay processes of the excited state molecule in the absence of external reactants. Because electronically excited molecules are highly energetic, they are susceptible to intermolecular reactions in which M* physically or chemically interacts with species in its environment (called quenchers, Q) (Balzani et al. 1975) to again return to ground state M or to another molecule P (see Figure 2b). When quenching processes are present, Equations (1) and (2) must be modified by adding $k_q[Q]$ to their denominators,

$$I \sim \Phi_e = \frac{k_r}{k_r + k_{nr} + k_q[Q]} , \qquad (3)$$

$$\tau = \frac{1}{k_r + k_{nr} + k_q[Q]} , \qquad (4)$$

where k_q is the quenching rate constant and the concentration of the reacting partner [Q] accounts for the bimolecular nature of the quenching process. It follows from this formalism that quenching pathways are dissipative and their presence will diminish the luminescence intensity and shorten the excited state lifetime. The Stern-Volmer relation quantitatively defines the attenuation in luminescence lifetime and intensity under quenching conditions as

$$\frac{I_o}{I} = \frac{\tau_o}{\tau} = 1 + \tau_o k_q[Q] , \qquad (5)$$

where I_o, I, and τ_o, τ are the luminescence intensity and lifetime in the absence and presence of Q, respectively. Owing to the short lifetimes of singlet excited states, significant concentrations (typically 0.01 molar or greater) of Q are required for quenching fluorescence. This is not the case for phosphorescence. The long lifetimes of phosphorescent excited states makes them especially susceptible to quenching at extremely small concentrations of Q.

Most of the imaging techniques based on molecular tagging may be understood in the context of the simple relations defined by Equations (1) – (5). Below is a description of the chemistry behind these techniques.

2.1 The Different Mechanisms of MTV

The four basic mechanisms that encompass current MTV techniques are shown in Figure 3. Sometimes referred to as Laser Induced Photochemical Anemometry (LIPA), mechanism A describes measurements based on the image produced by a photochromic dye and is the only MTV technique that relies on measuring absorbance. Light excitation produces a high-energy form of the dye, which usually is more strongly absorbing than the ground state molecule M (usually from transparent to opaque); the dye molecules in the flow are therefore tagged by the darkened image. Mechanism B describes the Raman excitation plus laser-induced electronic fluorescence (RELIEF) technique. In the RELIEF experiment, a high-energy form of the molecule, M´ (specifically vibrationally excited oxygen), is also responsible for creating the image. But unlike LIPA, M´ emits photons upon subsequent irra-

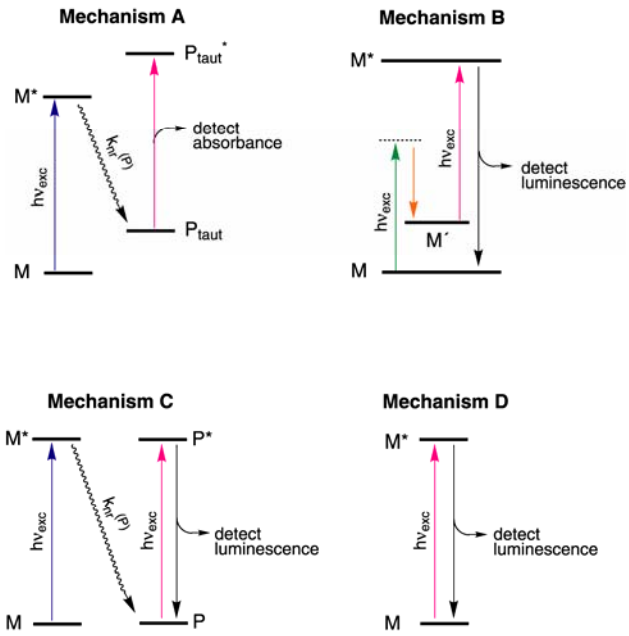

Fig. 3. The different mechanisms of MTV. M and M* designate a molecule in its ground and electronic excited state, respectively, and P indicated the formation of a new molecule. Consistent with Figure 2, solid arrows describe radiative transitions and wavy arrows indicate nonradiative transitions. The excitation lines are color coded to emphasize the number of different frequencies typically needed for each experiment. The different diagrams summarize the photochemistry and photophysics that give rise to the various MTV techniques under the various acronyms of LIPA based on photochromism (Type A), RELIEF (Type B), PHANTOMM, OTV, HTV (Type C), and direct luminescence (Type D).

diation. The RELIEF image is therefore revealed by detecting luminescence rather than absorbance. Mechanism C relies on the production of a luminescent molecule P upon excitation of a ground state molecule M. For the technique with the moniker photo-activated non-intrusive tracing of molecular motion (PHANTOMM), a laser dye is produced. Variants of the technique arise from the production of different P species: ozone in the Oxygen Tagging Velocimetry (OTV) technique, hydroxyl radicals in the Hydroxyl Tagging Technique (HTV) and two techniques based on the photorelease of NO. In each case, a luminescent image is produced upon excitation with a "write" laser and the image is detected by irradiating with a subsequent "read" laser pulse. Within mechanism C we also include the reverse approach such as photobleaching where, instead of releasing a luminescent tracer, a non-luminescent species is produced from fluorescent dyes, thereby creating a "negative" image. Mechanism D is the most straightforward of the MTV tech-

niques. An excited state molecule M* is produced by excitation. An image is detected by directly monitoring a long-lived phosphorescence from M* upon its radiative return to its ground state M. Details of each of the MTV techniques are presented next.

2.1.1 Mechanism A: MTV by Absorbance

Originally introduced by Miller (1962) for visualizing flows, photochromic chemicals were extensively used first by Hummel and his group for velocity measurements (Popovich and Hummel 1967; Frantisak et al. 1969; Hummel 1976; Ojha et al. 1989) and subsequently were more thoroughly applied to the MTV technique by Falco and Chu (1987) under the acronym LIPA (Laser Induced Photochemical Anemometry). In a photochromic process, laser excitation of molecule M produces an electronically excited molecule M*, which then relaxes by nonradiative decay ($k_{nr}^{(M)}$ and $k_{nr}^{(P)}$). Whereas most of the vibrational energy is released as heat ($k_{nr}^{(M)}$), some vibrational energy is channeled into the making and/or breaking of bonds ($k_{nr}^{(P)}$) to produce a high-energy form of the molecule, P_{taut}; in chemical terms, this high-energy molecular species is called a tautomer (the same molecular framework connected by a different bonding pattern). This tautomeric process is adaptable to MTV because the absorption spectra of M and P_{taut} are different. The color change accompanying the M to P_{taut} conversion can be detected by exciting with a white light source. In the context of MTV description, the long lifetime tracer in this case is the newly produced P_{taut}, which can persist for several seconds to minutes.

The photochromism of commercially-available substituted benzyl pyridines and spiropyran dyes have been used for most velocimetry measurements to date. The structure of these dyes and their overall photochemistry are depicted in Figure 4. The nature of the X_i substituent on either tracer may be varied to tune the precise spectroscopic and photophysical properties of the dye. In the benzyl pyridine and spiropyran systems, M is colorless to slightly yellow whereas P_{taut} is dark blue. This color change results from the increased conjugation (the alteration of single and double bonds) of the molecular framework upon conversion to the high-energy tautomer. For the molecules on the left side of Figure 4, electrons in the π system of the dye (those electrons associated with the alternating single and double bonds) are confined to a single six-membered ring (highlighted by the dark outline). Excitation to M* followed by subsequent nonradiative decay causes the making and breaking of bonds such that the π system is extended. The increase in the conjugation allows the electrons to delocalize over a longer part of the molecule, resulting in a red shift of the absorption spectrum from the ultraviolet to the visible spectral region as explained by quantum mechanical particle-in-the-box formalisms (Merzbacher 1970). Use of photochromic chemicals requires two photon sources. When solutions of the photochromic tracers are irradiated with a "write"laser, typically a UV laser (e.g. 351 nm wavelength), P_{taut} is produced and an opaque image is generated along the path of excitation. A second light source (usually a white light source) is then needed to see or "read" the image.

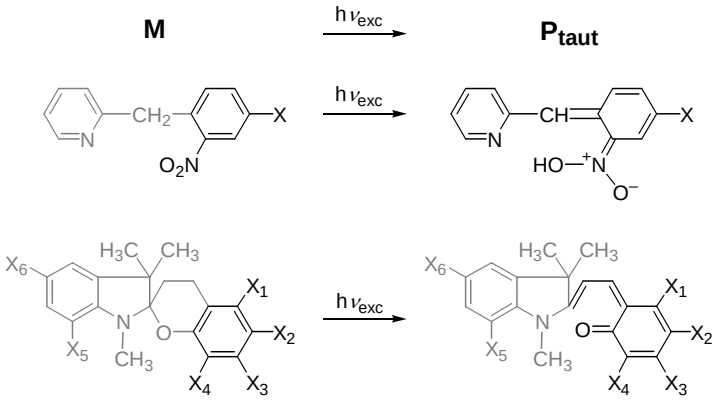

Fig. 4. Photochemical transformations of two popular photochromic dyes used for MTV: the substituted benzyl pyridines (top) and spiropyran dyes (bottom). The molecules are labeled with respect to the M and P_{taut} designations of Figure 2 (Mechanism A). The bold lines show the molecular framework responsible for the color change upon laser excitation.

There are several advantages of molecular tagging by a photochromic tracer. The nonradiative conversion from M* to P_{taut} occurs rapidly, within the duration of a nanosecond laser pulse, and hence the image is formed promptly upon laser irradiation. The conversion of P_{taut} back to M occurs reversibly so the tracer is reusable. Moreover, P_{taut} persists for several seconds to minutes before thermally converting back to M. Thus, flows moving at slow speeds may be studied and the photochromic tracer can be repetitively used. Though yet to be implemented in fluid flow studies, there are numerous other photochromic imaging systems offering a wide range of available chemical and spectroscopic properties. A purported drawback of this mechanism is the insolubility of these photochromic dyes in water. While it is true that most all studies using photochromics have been performed in organic liquids (typically kerosene), relatively minor chemical modifications to many photochromic dyes would enable them to easily dissolve in water (Yurechko and Ryazantsev 1991).

Despite these advantages (i.e. long lifetime, reusable), there is one drawback of photochromic systems that limits their overall utility for MTV. Because the image is produced by a change in absorbance, the difference between incident and transmitted light must be measured, a task which greatly complicates data collection and analysis. Indeed, emitted light (against a black background) is more easily and accurately detected than transmitted light and consequently images based on luminescence are more amenable to MTV. For this reason, the major advances in the MTV technique in recent years have been made with the luminescence-based imaging schemes of mechanisms B, C and D. Nevertheless, MTV with photochromics have been used effectively in fluid dynamics studies (e.g. D'Arco et al.

1982; Falco and Chu 1987; Chu and Liao 1992; Chu et al. 1993; Zalzal et al. 1994; Chu et al. 1995; Couch et al. 1996; Park et al. 1999).

2.1.2 Mechanism B: MTV by Vibrational Excited State Fluorescence

The Raman excitation plus laser-induced electronic fluorescence (RELIEF) technique was designed by Miles and co-workers (Miles et al. 1987; 1989a,b; 1993; 1997) for molecular tagging in unseeded air flows. The technique is schematically described in Figure 3 (Mechanism B). The oxygen in the air flow is tagged by a laser to produce oxygen in a vibrational excited state, which is long-lived and its displacement can subsequently be interrogated, or "read", by exciting to an electronic excited state that is emissive. The mechanism is ingenious in its design because the long lifetime tracer needed to follow the flow is derived from the vibrational excited state of oxygen; the short-lived fluorescence of the electronic excited state of oxygen is used to only interrogate the vibrationally excited molecule.

RELIEF is the most spectroscopically sophisticated MTV technique. The spectroscopic underpinning of RELIEF is based on the stimulated Raman effect (Long 1977), which is familiar to most as a method to Raman-shift the wavelength of light from a laser pump source. In normal Raman scattering, laser irradiation of frequency ν_o results in the spontaneous population of a vibrational excited level. The populations are small, however, and vibrational excited states are not produced in sufficient concentration to be viable for velocimetry. At high laser irradiances (electric fields of $>10^9$ V m^{-1}) nonlinear effects will dominate such that a substantial fraction of the exciting radiation of frequency ν_o is converted into radiation of frequency $\nu_o \pm n\nu$, where ν is the vibrational frequency of the molecule. Most of the power (sometimes as much as 50%) is transferred to the first Stokes line, $\nu_o - \nu$. In the context of Figure 3, the exciting, nonlinear radiation $\nu_o - \nu$ pumps the system from its ground to its first vibrational level by driving the system through a virtual excited state (indicated by the dashed lines). For oxygen, the process involves the population of the first vibrational level ($\upsilon = 1$) of the $^3\Sigma_g^-$ electronic ground. The formation of the long lifetime tracer, i.e. the vibrationally excited oxygen, is rapid and occurs within the laser pulse of order 10 ns. This vibrational level can be very long-lived, approaching 27 ms at 1 atm (Frey et al. 1972). However, for MTV applications, the usable lifetime is in the 100-microsecond range owing to collisional deactivation of vibrationally excited oxygen by water and carbon dioxide (McKenzie 1993). In most applications to date, the time delay between tagging and interrogation has been of order 10 μs or less. From the $^3\Sigma_g^-$ ($\upsilon = 1$) vibrational excited state, oxygen can be excited to its $^3\Sigma_u^-$ (or sometimes referred to as the B) excited state (responsible for the famous Schumann-Runge bands of oxygen (Herzberg 1950) from which 200-400 nm fluorescence may be observed for interrogation purposes.

The requirement of three frequencies (i.e. two to tag, one to interrogate) makes the RELIEF technique challenging to implement. The power transferred to the

first Stokes line at $\nu_o - \nu$ is related exponentially to the incident laser power. The intense light at the difference frequency needed to produce sufficient concentrations of the vibrationally excited oxygen is provided by mixing the 532-nm 2nd harmonic of a Nd:YAG laser and the 580-nm output of a dye laser, or a Raman cell frequency shifter, also driven by the 532-nm line of the same Nd:YAG laser. For interrogation, the 193-nm output of an ArF excimer laser is needed to promote the vibrationally excited oxygen molecules into the fluorescent Schumann-Runge manifold. On the detection side of the experiment, the overall imaging of the flow is complicated by the fact that the $^3\Sigma_u^-$ fluorescent excited state of oxygen is predissociative leading to the homolytic cleavage of the oxygen-oxygen bond (Feast 1948). Bond cleavage is of course a nonradiative decay process, hence the overall quantum efficiency for fluorescence is small. In addition, the electronic communication between excited and ground states is poor (owing to poor Franck-Condon factors) so that the efficiency for fluorescence is further compromised. Despite these challenges, MTV measurements with RELIEF have been successfully carried out in gas phase, oxygenated flows (e.g. Miles et al. 1993; Noullez et al. 1997; Miles et al. 1989a,b; 2000).

2.1.3 Mechanism C: MTV by Photoproduct Fluorescence

The photo-activated nonintrusive tracking of molecular motion (PHANTOMM) is based on tracers that would otherwise luminesce if not for the attachment of a deactivating, or caging, group. First introduced by Lempert et al. (1995) for liquid phase flows, the overall technique relies on two sources of photons. Laser excitation leads to the photolytic removal of the deactivating group to produce a fluorescent dye with high emission quantum efficiencies. In the context of MTV description, the long lifetime tracer in this case is the uncaged laser dye, which can persist for a very long time. The laser dye is spatially produced only where the "write" laser has excited the flow. The displacement of the tagged regions is revealed by illuminating the flow with a "read" laser to reveal the fluorescence from the uncaged dye. The uncaged dye can be tracked indefinitely since the photolytic removal of the deactivating group is irreversible. For this reason, the PHANTOMM technique can accommodate very slow flow speeds and has been utilized in several novel applications (e.g. Harris et al. 1996a,b; Biage at al. 1996; Paul et al. 1998; Lempert and Harris 2000b; Park et al. 2001; Sinton et al. 2004).

An obvious question is why does the laser dye need to be photogenerated in the first place? Returning to the discussion of Section 2, fluorescence is short-lived; thus a fluorescent image that is directly produced by laser excitation will exist for only 1-10 ns. The glowing image is too short-lived to lead to sufficient displacement over the convection timescale of most flows. The PHANTOMM technique overcomes this limitation by uncaging the fluorescent dye. From a chemical perspective, PHANTOMM is the luminescent counterpart to LIPA. In both techniques, an initial excitation pulse is used to produce a tracer, which can be followed in time; with LIPA the tracer is absorbing and hence tracked by the detection of transmitted light, whereas in PHANTOMM the tracer is tracked by detecting emitted light.

The detection of a fluorescent image offers several advantages to the PHANTOMM technique. Because the transition between the singlet excited state and singlet ground state is allowed for strongly absorbing materials such as organic laser dye molecules, k_r approaches 10^9 sec^{-1}. This rate of radiative relaxation is so large that the nonradiative decay channels k_{nr} are generally not competitive (i.e. $k_r >> k_{nr}$). From Eq. 1, the emission intensity of the PHANTOMM image is therefore intense. Also because fluorescence lifetimes are short (on the order of ~ 1 - 10 ns, see Eq. 2), the excited state (and hence the tagged region in the PHANTOMM technique) is not readily quenched by oxygen. This can be understood within the context of Eq. 5. The quenching rate for oxygen is diffusion controlled (i.e. $k_q = 10^9$ $M^{-1}s^{-1}$), and its concentration in solution is typically 10^{-3} M. With an excited state lifetime of ~ 10^{-9} s^{-1}, a maximum quenching of 0.1% will be observed. Thus the fluorescence image is not affected by air, a fact long known to the practitioners of Laser Induced Fluorescence (LIF). The short lifetime of the fluorescence of uncaged dye offers another significant advantage for increasing signal gain. Once uncaged, a dye can be excited multiple times, allowing for multiple photons to be detected from an individual activated dye over time durations that are short with respect to fluid motion. Lempert et al. (1995) have estimated that the photogenerated fluorescein dye (with its natural radiative lifetime of 4.5 ns and quantum yield of 0.90) can emit 150 photons over the duration of a conventional flashlamp-pumped dye laser (FWHM = 2 μs), which is a time scale that is frozen with respect to fluid motion in most liquid applications.

A variety of caged fluorescent dyes is currently available commercially from Molecular Probes, Inc (Eugene, Oregon, USA). Two such tracers are shown in Figure 5. In each case the dye is modified with a methoxynitroaromatic deactivating, or caging, group. The covalent attachment of the deactivating group renders the latent fluorescent dye non-emissive. The tracers can be activated with the third harmonic of a Nd:YAG laser (355 nm) to produce dyes with luminescence properties of fluorescein and pyrene. Though the precise mechanism for the photolytic removal of the deactivating group has yet to be determined, it likely occurs via well-known resonance structures involving the nitro group to yield an aldehyde through a photochemistry that appears to be initiated by π to π^* excitation of the deactivating group (McCray and Trentham 1989). However, even though the excitation light may be absorbed within the appended group, it cannot be contained there and it is free to flow to all bonds in the molecule on vibrational time scales (subpicoseconds). The non-specificity of the excitation process means that the photolytic removal of the group does not occur immediately upon laser excitation; specifically, the deactivating group falls off of the dye on millisecond time scales (Lempert et al. 1995), which establishes the upper limit for the flow speeds that can be investigated. Moreover, as emphasized in Figure 5, the luminescent dye is produced irreversibly by cleavage of a covalent bond. Thus the overall tracer can be used only once. A significant advance to the overall approach will be creation of photoactivated dyes that can be uncaged promptly and reversibly.

Interestingly, the PHANTOMM concept, though not so named at the time, was first implemented by Boedeker (1989), and further utilized by Goss et al. (1991), using a much simpler tracer molecule than those shown in Figure 5. Water will

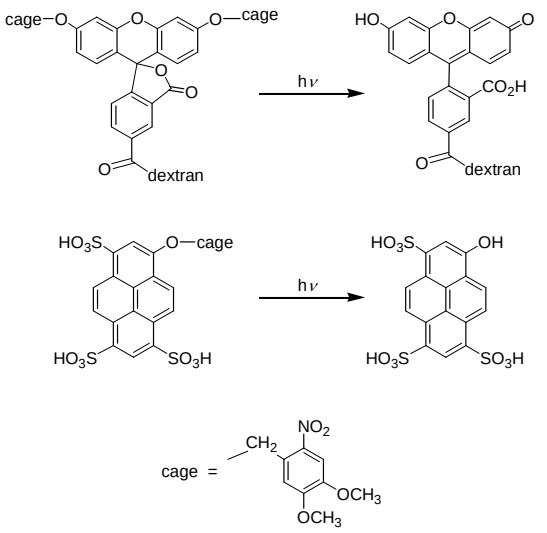

Fig. 5. Chemical structures of two PHANTOMM tracers before and after photolytic cleavage of the deactivating group. The photochemistry of the top caged tracer produces a fluorescein dye, whereas that of the bottom caged tracer yields a pyrene fluorophore.

photodissociate to OH and H radicals upon two photon excitation at 248 nm (Meijer et al. 1986). Subsequent excitation with a second laser at 308 nm yields the fluorescence characteristic of the Q_1 transitions (Exton and Hillard, 1986) of the OH radical. With regard to the PHANTOMM construct, the caged tracer is water, the deactivating group or cage is an H radical, and the fluorescent dye is the OH radical. The need for two-photon excitation to release the OH radical makes the technique difficult to implement. Nevertheless, Boedecker's approach permits gas phase flows to be imaged by the PHANTOMM technique with the caveat that the OH radical tracer has a short lifetime and thus is restricted to high-speed flows. Related studies by Goss et al. (1992) have expanded Boedeker's approach to permit high speed, combusting, flows to be imaged by luminescence from C, C_2 and CN tracers produced by the photolysis of hydrocarbons.

Under the acronym Hydroxyl Tagging Velocimetry (HTV), Pitz and coworkers have advanced the use of OH radical fluorescence by replacing the two-photon "write" pulse with a one-photon pulse (Wehrmeyer et al. 1999a,b; Pitz et al. 2000; 2005; Ribarov et al. 2002; 2004). In this adaptation, single-photon dissociation of vibrationally excited water molecules to produce the OH radical is achieved by the 193-nm excitation wavelength of an ArF excimer laser. The tagged regions are imaged with the OH radical fluorescence excited by the 248-nm wavelength of a KrF excimer laser. Though not yet implemented, the 308-nm excitation frequency of a XeCl excimer laser should also be suitable to image the OH radical fluorescence. The technique has been used to image the flow fields of

combusting H_2-air flames. At lean concentrations of H_2, OH radical lifetimes approach 1 ms. For rich H_2 flames, however, the lifetime of the OH radical drops to ~200 ns owing to its reaction with H_2 to produce H_2O and H radical. The advantage of the single photon generation of OH radical from H_2O is that larger spatial regions can be tagged with single photon excitation. HTV has recently been used in a non-combusting supersonic flow where water was sprayed upstream to provide moist air and adequate OH signal level (Pitz et al. 2005).

In the Ozone Tagging Velocimetry (OTV) technique of Pitz and co-workers (Pitz et al. 1996; 2000; Ribarov et al. 1999) the "caged-dye" is ozone, which is created from oxygen O_2 by the same reaction chemistry that produces ozone in the upper atmosphere. The basic photochemistry of the OTV technique is shown below:

$$O_2 + h\nu\ (\lambda = 193\ \text{nm}) \rightarrow O(^3P) + O(^3P)$$
$$O(^3P) + O_2 \rightarrow O_3$$
$$O_3 + h\nu\ (\lambda = 248\ \text{nm}) \rightarrow O(^3P) + O_2^*$$
$$O_2^* \rightarrow O_2 + h\nu_{fluor}$$

Two sources of photons are therefore needed for this approach. The 193-nm light from an ArF excimer laser impinging on air causes oxygen to dissociate into two oxygen radicals. These $O(^3P)$ radicals react with undissociated oxygen to produce ozone, O_3, which is the long lifetime tracer and the tagging reagent. After a known delay time, the position of the O_3 tag line is revealed by the application of a 248-nm pulsed laser sheet produced from a KrF excimer laser. The 248-nm excitation undoes the chemistry of the 193-nm laser line, causing ozone to photodissociate to an $O(^3P)$ radical and O_2, which fluoresces via the Schumann-Runge transitions that are accessed by the KrF interrogation laser. The long imaging lifetimes are derived from the ozone tracer, which is stable in air at room temperature. However, at increased temperatures, ozone is unstable with respect to thermal decomposition; thus, the OTV technique is not suitable for hot flows (e.g. beyond 600 K). In addition, the formation of O_3 from O_2 with the 193-nm laser pulse is not rapid and occurs over a time scale of ~20 μs. In a situation similar to the uncaging of fluorescein in the PHANTOMM technique, the delay between laser tagging and the generation of enough ozone to obtain a fluorescent image with sufficient signal/noise ratio dictates the fastest flow speeds that can be accommodated.

Another tracer molecule that can be produced from uncaging is nitric oxide, NO. The fluorescence of NO has long been used in LIF measurements (MacKenzie, 1993). As with all the techniques of this section, implementation of the tracer for MTV applications requires its generation from a parent molecule. Whereas many other small molecular tracers exhibit only short lifetimes due to energy transfer processes or high reactivity, NO is stable on the millisecond time scale, thus allowing for relatively slow flows to be imaged. There are two caged NO molecules that have been employed to date for this MTV mechanism. NO_2 may be dissociated in the focused beam of a 308-nm XeCl laser (Orlemann et al. 1999). The generated NO may be imaged by the fluorescence of NO, generated by its excitation with a Raman-shifted 226-nm line from a KrF excimer laser. NO may also be generated from tert-butyl nitrite that is seeded in an air or nitrogen

flow (Krüger and Grünefeld, 1999; 2000). NO is released upon excitation with either a 193-nm ArF laser or a 248-nm KrF excimer laser. The photodissociation cross-section of the tert-butyl nitrite at 248 nm is a factor of ~2 smaller than compared to 193 nm, but the pulse energies of the KrF lasers are generally higher. Finally, NO may be generated by irradiating air with an intense laser beam (under the moniker APART – Air Photolysis And Recombination Tracking) (Dam et al. 2001; Sijtsema et al. 2002; van der Laan et al, 2003). The tracer results from the creation of NO from reaction of N_2 and O_2 in the field of illumination of a focused ArF excimer laser beam (193-nm wavelength). This MTV scheme is attractive because the air flow may be imaged without any kind of seeding.

A different implementation of mechanism C for MTV applications relies on the laser-enhanced ionization (LEI) of an atomic species present naturally in the flow or seeded into it (Barker et al. 1995). The LEI technique relies on exciting a neutral atom or molecule to an excited state near its ionization limit. A second photon can then be used to ionize the atom or molecule, thus producing a depletion of the neutral species, which is typically fluorescent. The detected region is revealed by an attenuation of luminescence intensity. Pertaining to the mechanism described in this section, the LEI technique yields a "negative" image as compared to the foregoing techniques of this section. Instead of releasing a luminescent tracer, the ionizing laser pulse produces a non-luminescent species. Detection of a quenched luminescence against a bright background complicates the implementation of MTV and limits the overall dynamic range of the technique. Most recently, the LEI technique has been improved by using the secondary laser to produce a luminescent image (Rubinsztein-Dunlop et al. 2001). In this implementation, neutral strontium ions seeded into a flame are ionized by first resonantly exciting (λ_{exc} = 460.733 nm) neutral strontium atoms from their ground state ($5s^2$, $^1S_0$) to a Rydberg state ($5s^15p^1$, $^1P_1$), followed by subsequent ionization of this excited species to produce strontium ions with the 308-nm output of an excimer laser. Fluorescence from the strontium ions is detected at 407.8 nm upon excitation with a 421.552 nm "read" laser pulse. The precise excitation frequencies are produced from XeCl-pumped dye lasers. The technique is somewhat cumbersome to implement as two pump and two dye lasers are needed to produce the fluorescent image; one laser system for the production of the strontium ions and another to produce the laser-induced fluorescence image. The short lifetime of strontium ions (of the order of 60 μs due to ion-electron recombination processes) makes this approach suitable for imaging supersonic and hypersonic flows.

Yet another alternate implementation of mechanism C includes a photobleaching approach. Continuous excitation of organic dyes reduces the ability of the dye molecules to absorb photons and emit fluorescence, thereby reducing the effective concentration of active dye molecules and a reduction of fluorescence emission from the bleached regions. The detrimental effects of photobleaching have been previously addressed in quantitative LIF studies (Koochesfahani 1984; Crimaldi 1997; Wang and Fiedler 2000). A first order description of the photobleaching process defines the bleaching effectiveness in term of a rate that is proportional to the excitation source photon flux and properties of the dye molecule, i.e. absorption cross section and bleaching quantum efficiency (Koochesfahani 1984). As a

result, effective photobleaching over a short timescale requires a high intensity laser source. In comparison with the PHANTOMM concept, this is a reverse approach where, instead of releasing a luminescent tracer, a non-luminescent species is produced from fluorescent dyes, thereby creating a "negative" image. As already described previously, however, detection of reduced luminescence against a bright background complicates the implementation of MTV and limits the overall dynamic range of the approach. Nevertheless, MTV measurements based on photobleaching have been successfully carried out (e.g. Rička 1987; Schrum et al. 2000; Mosier et al. 2002; Wang 2005).

2.1.4 Mechanism D: MTV by Direct Phosphorescence

Molecular tagging based on direct photoluminescence is the easiest technique to implement. A single laser is used to produce a luminescent excited state, which is extremely long-lived and its displacement by the flow can be imaged by simply monitoring the emanating luminescence. In the context of MTV description, the long lifetime tracer in this case is the excited state molecule itself. The emission of a photon returns the molecule back to its ground state where the tracer may be re-excited; thus the tracer is re-usable.

The overall approach of the MTV technique based on mechanism D is similar to LIF, but the tracer has a long enough lifetime to permit sufficient displacement of the luminescent tagged regions with the flow. The requisite long lifetimes of the tracer necessarily require the luminescence to be phosphorescence-based. This presents two obstacles to the development of MTV tracers for mechanism D. Successful imaging systems with long lifetimes must display the intrinsic property of a small k_r. But k_{nr} must be even smaller if the emission quantum yield is to approach its theoretical limiting value of unity (see Eqs. 1 and 2) and produce intense luminescence intensities. This requirement demands that efficient nonradiative decay pathways to be eliminated in the design of imaging reagents. However, this property does not necessarily ensure a viable MTV technique; even if k_{nr} remains small with regard to k_r, long-lived excited state molecules have enough time to react with other molecules in their environment by quenching. As discussed in the context of Equations (3) and (4), quenching leads to decreased emission intensity and lifetime, respectively.

For MTV applications based on mechanism D, quenching is an issue pervading most measurements. Water, oxygen, and residual metals in the environment are good quenchers of luminescence. As described by Equation (5), the lifetime and intensity of an excited state decrease with increasing concentration of these quenchers. Thus a primary challenge in the design of any successful imaging system is to minimize these quenching pathways. The most problematic quencher in engineering applications is oxygen, owing to its efficiency and prevalence in the environment. Oxygen quenches phosphorescent excited states by an energy transfer mechanism. The problems that oxygen brings to bear to the MTV technique can be explicitly demonstrated by considering Equation (5). Typically the quenching rate for oxygen is diffusion controlled (i.e. $k_q = 10^9\ M^{-1}s^{-1}$), and its concentration in solution is typically 10^{-3} M and in air is 10^{-2} M. According to Equation (5),

the lifetime and intensity of a tracer possessing an inherent 1 ms photoluminescence lifetime (τ_o) will be attenuated by 10^3 in oxygenated solutions and will be reduced by over 10^4 in air.

Indeed, in the absence of oxygen, MTV measurements can be performed with a variety of organic phosphors. Some of the popular tracers such as biacetyl and acetone, which have often been used for flow visualization and LIF concentration measurements, can also be used as MTV tracers. The potential of biacetyl for this purpose has been known for sometime (Hiller et al. 1984; Lowry 1987; Liu et al. 1988), and detailed multi-point measurements have been carried out with it (Hilbert and Falco 1991; Stier and Koochesfahani 1997;1998;1999; Hascher et al. 1998; Thurlow and Klewicki 2000; Goh 2001; Koochesfahani et al. 2004). Biacetyl (also called 2,3 butanedione) has a broad absorption spectrum with maxima at 270 and 420 nm. It is non-toxic and its relatively high vapor pressure (40 Torr at room temperature) allows a molar seeding of ~ 5%. Biacetyl phosphoresces with a high quantum yield (0.15) and with a lifetime approaching 1.5 ms in nitrogen and helium flows. Nevertheless, oxygen completely quenches the green phosphorescence of biacetyl, even when present in only trace levels, rendering it impractical for general use in oxygenated flows such as air. More recently, Lempert and coworkers have demonstrated the acetone-based MTV approach and applied it to high speed micro jet flows (Lempert et al. 2002; 2003).

Long-lived, unquenchable, tracers for MTV applications may be constructed by connecting small molecular subunits in intricate ways to lead to elaborate molecular architectures (Pikramenou et al. 1994; Mortellaro and Nocera 1996a,b; Nocera 1996). These supramolecules contain multiple sites of complementary function – at one site is a photoactive center capable of emitting visible light and at the other is a docking site for the photoactive center. The strategy centers on manipulating the fundamental parameters governing the luminescence intensity of a photoactive center such that molecular recognition of a constituent at the docking site causes k_r to be much greater than k_{nr} and k_q (Rudzinski and Nocera 2001). In this manner, it is possible to develop tracers with long-lived, bright phosphorescence that are not quenched.

Examples of such tracers are those based on lanthanide ions such as europium (Eu^{3+}) and terbium (Tb^{3+}) that have been developed for the study of two-phase flows. These ions exhibit luminescence from transitions involving electrons residing in orbitals buried deep within the ion. For this reason, the luminescent excited state is shielded from the external environment. Although oxygen will physically contact the lanthanide ion upon collision, it cannot communicate with the luminescent excited state owing to poor electronic coupling (Balzani et al. 1980; Endicott 1988) and oxygen quenching of lanthanide luminescence is not predominant. Yet water is an excellent quencher of lanthanide luminescence because its O—H bonds act as good thermal receptacles for the excited state energy of lanthanide-based active sites (Horrocks and Albin 1983). The deleterious effect of water can be circumvented by encapsulating the lanthanide ion in a molecular cage – a cryptand ligand (see Figure 6). The two nitrogens and five oxygens comprising the three straps of the 2.2.1 cryptand ligand occupy seven of the nine coordination sites of the lanthanide ion; the two remaining coordination sites are important for

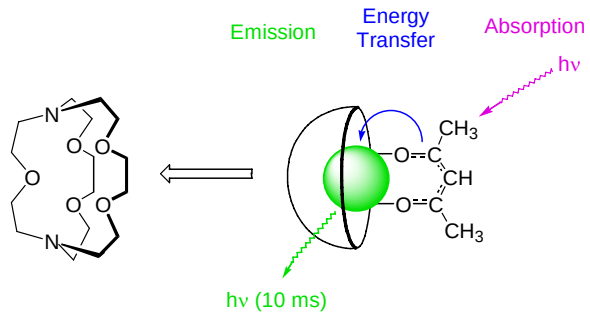

Fig. 6. A cryptand molecular cage encapsulates the photoluminescent Tb^{3+} ion (indicated by shaded ball) with two remaining coordination sites occupied by light-harvesting groups, thereby allowing the photoactive Tb^{3+} center to be indirectly excited.

docking a light-harvesting group described below. The excited states of lanthanide ions are intrinsically bright lumophores, but they show little or no luminescence under direct irradiation because the excited states are spin-forbidden, and therefore they have low absorbance (Bünzli 1988). Docking or coordination of a light-absorbing group like acetylacetonate (acac) at the two unoccupied coordination sites opens up a conduit for energy to flow from the light-harvesting group to the lanthanide ion (Yu et al. 1991) and results in the green luminescence of the Tb^{3+} ion, which subsequently decays with its natural lifetime of 1.7 ms. This absorption-energy transfer-emission process (Balzani and Scandola 1991) allows the lanthanide ion to indirectly be excited with intensities 10^3-10^4 times greater than in its absence. Thus this tracer emits brightly, possesses a long lifetime and its excited state is not quenched by oxygen or water. These properties have allowed a successful implementation of this tracer in a study of two-phase flows by the MTV technique (Falco and Nocera 1993).

Interest in developing tracers with even longer lifetimes has led to a class of supramolecules called cyclodextrins (CDs). Cyclodextrins are cyclic oligosaccharides (Wenz 1994), formed from connecting six, seven, or eight D-glucose rings (a common sugar) in a head-to-tail arrangement (α-, β-, and γ-, respectively), see Figure 7. The molecule is cup-shaped with its size determined by the number of sugars in the structure. The CD most often used in MTV applications (see Gendrich et al. 1997) is β-CD, which is constructed from seven sugar subunits, resulting in an outer cup dimension of 15.3 Å and an inner cup dimension of 7.8 Å. Hydroxyl groups of the sugar rings encircle the outer rims of the CD cup, imparting water solubility. To increase the solubility even more, an additional glucosyl subunit is hung off of the rim (called Gβ-CD). The hydrocarbon rings of the D-glucose subunits of the cup walls define a water-repelling or hydrophobic interior that allows it to absorb water-insoluble or hydrophobic compounds. Thus the cyclodextrin is a miniature bucket that dissolves in water but will fill itself with hydrophobic compounds.

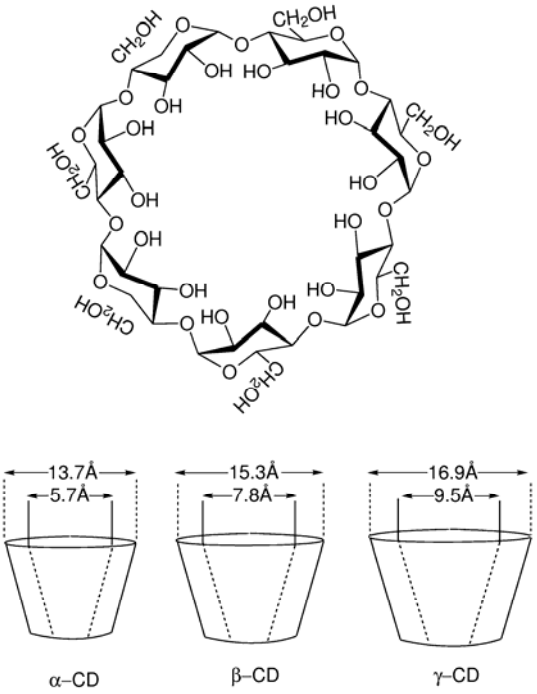

Fig. 7. A cyclodextrin and the dimensions of the CD cup for the α, β, and γ forms.

The CD cup can be filled with a lumophore such as 1-bromonaphthalene (1-BrNp). This molecule has a bright fluorescence with a 9 ns lifetime. The purpose of attaching the bromine to the molecule is to induce a crossing from fluorescing, singlet excited state to a triplet excited state. The bright green phosphorescence (10 ms is the natural lifetime but the lifetime may decrease to ~5 ms when intense irradiation sources are used) from 1-BrNp is efficiently quenched by oxygen, even when the lumophore is included within a CD cup, as shown in Figure 8 (spectrum A) only the short-lived blue fluorescence of the 1-BrNp is observed. The phosphorescence can be recovered when certain alcohols (indicated collectively by "ROH") are added to the solution. Exhaustive equilibria, photophysical, and kinetics studies for a series of alcohols (Ponce et al. 1993) reveals that a ternary complex (1-BrNp•Gβ-CD•ROH) is formed among the alcohol, CD and 1-BrNp. The mechanism that gives rise to the triggered phosphorescence by alcohols is shown in Figure 8. In short, the alcohol hydrogen bonds to the rim of the CD cup, and the aliphatic end of the alcohol flips over the hydrophobic interior of the CD. Accordingly, the alcohol acts as a lid for the CD cup thereby shielding 1-BrNp from oxygen (see Figure 9). Phosphorescence enhancements can be very large, approaching 10^4-10^5, depending on the fit of the alcohol lid to top of the CD cup (Hartmann et al. 1996).

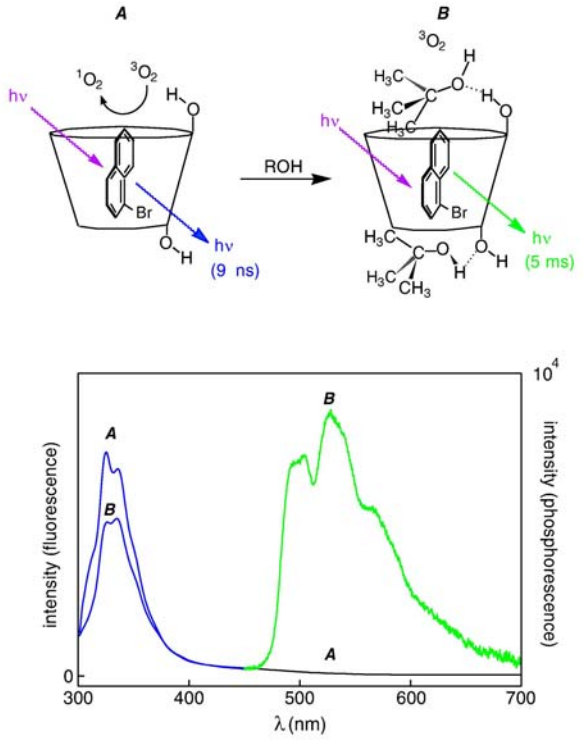

Fig. 8. Phosphorescence from 1-bromonaphthalene (1-BrNp) included within a CD is observed only when alcohols are present. In the absence of alcohol (A), only blue fluorescence is observed. Green phosphorescence is triggered upon addition of an alcohol such as tert-butanol (B).

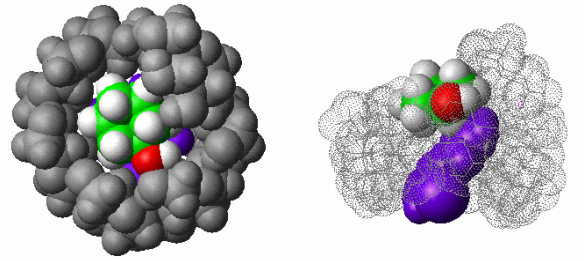

Fig. 9. Top and side views of computer-generated molecular mode of the tracer from 1-BrNp, CD and cyclohexanol. The CD is speckled in the side view so that the inside of the cup may be viewed. The purple molecule is the 1-BrNp and the multi-colored molecule is the cyclohexanol. In the top view, the cyclohexanol obscures the 1-BrNp. It is this "blocking action" that prevents oxygen from quenching the phosphorescence of the 1-BrNp.

The details of the MTV implementation and other applications of the phosphorescent supramolecules described above are found in Gendrich et al. (1997). The choice of the alcohol and its concentration strongly influence the phosphorescence lifetime and intensity. For MTV studies, cyclohexanol and neopentanol are the alcohols of choice, and the excitation sources used to date are the 308-nm of the XeCl excimer laser or the 266-nm of quadrupled Nd:YAG. Since phosphorescence emission is produced only when all components (Gβ-CD, 1-BrNp, and alcohol) of the ternary complex are present, it is possible to devise in addition to pure velocimetry other applications for molecular tagging passive scalar mixing regions, or chemical reaction interfaces, and monitor their Lagrangian evolution. In more recent studies (Hu et al. 2006; Hu and Koochesfahani 2006) the original glucosyl sub-units (i.e. in Gβ-CD) have been replaced by maltosyl sub-units (i.e. Mβ-CD). The measured properties of both glucose- and maltose-based triplexes are quite similar and the two can be used interchangeably. The three components of these phosphorescent complexes are commercially available; the various alcohols and the lumophore (1-BrNp) are readily found in catalogs of most scientific chemical companies, and maltosyl beta CD is available from Cyclodextrin Technologies Development, Inc. (Gainesville, Florida, USA) under the trade name Trappsol.

3. The Experimental Implementation of MTV: Tagging Methods, Detection and Processing

The specific complexities in the photophysics of the various molecular tracers used for MTV determine the wavelength and number of photon sources needed for tagging and those needed for interrogation. Regardless of these complexities, implementation of MTV for fluid flow studies involves certain common issues that are discussed in this section.

3.1 Tagging Methods

Molecular tagging along single or multiple parallel lines is the simplest method of tagging and has been utilized in a large fraction of MTV studies to date. The experiment is typically configured to create tagged lines perpendicular to the primary flow direction and the velocity is estimated from the displacement of these lines. Two examples of single-line tagging are shown in Figures 10 and 11. Figure 10 depicts the displacement of a tagged line that is created by RELIEF (MTV mechanism B) in a turbulent air jet. The resulting velocity data have been used to elucidate certain characteristics of turbulent velocity fluctuations (Noullez et al. 1997). Figure 11 illustrates the image pair from single-line tagging using caged fluorescein (MTV mechanism C). These image data have been used to characterize the internal circulation inside a falling water droplet (Harris et al. 1996; Harris

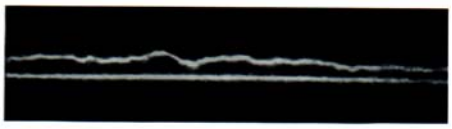

Fig. 10. Typical single-line RELIEF image pair taken in a turbulent free air jet with 0 μs (lower line), and 7 μs (upper line) time delay (Noullez et al. 1997). The line is approximately 1.2 cm long.

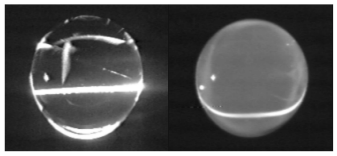

Fig. 11. Single-line tagging image pair inside a free falling 5-mm diameter water droplet using caged fluorescein (Harris 1999). Time delay between initial tagging (left) and displaced image (right) is 29.5 msec

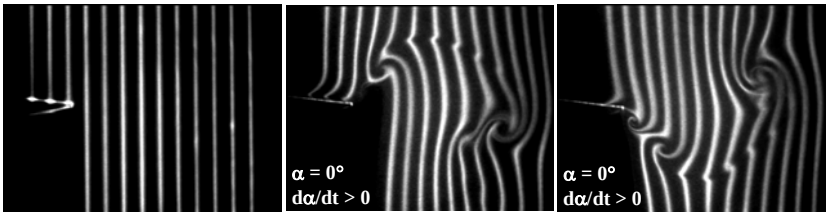

Fig. 12. Multi-line tagging in the trailing region of a NACA-0012 airfoil pitching sinusoidally with an amplitude of 2 degrees (Koochesfahani and Bohl 2002). The tagging pattern (left image) right after the laser pulse is a series of parallel lines with a spacing of 3 mm (about 0.025 chord length). The displaced lines are shown at zero angle of attach during pitch-up (middle image) and pitch-down (right image).

1999). An example of multi-line tagging using phosphorescent supramolecules (MTV mechanism D) in a water tunnel is provided in Figure 12. This figure illustrates the trailing edge region of a NACA-0012 airfoil oscillating sinusoidally at a high reduced frequency of $k = 8.8$ and amplitude of 2 degrees (Koochesfahani & Bohl 2002). The time delay between tagging and interrogation is selected to be long (about 20 ms) to allow a large displacement of the tagged lines so that the flow patterns caused by vortical structures and vortex sheets can be easily observed.

When using line tagging, it is important to recognize that this tagging method allows the measurement of only one component of velocity, that normal to the tagged line. In addition, the estimate of this velocity component has an inherent error associated with it, which is connected with the ambiguity in the unique determination of the displacements of various portions of a (continuous) tagged line. Following the analysis of Hill and Klewicki (1996), the error can be written in the form $\Delta u / u = (\upsilon / u)(\partial u / \partial y)\Delta t$, where u is the estimated velocity component normal to the tagged line, Δu is the error in the estimated velocity, υ is the flow velocity component parallel to the tagged line, and Δt is the time delay between tagging and interrogation. Clearly an *a priori* knowledge of the flow field is nec-

essary in order to provide an estimate of the error. It can be observed, however, that this inherent error is identically zero only in flows where the velocity component v along the tagged line is zero (i.e. unidirectional flows) or where the velocity gradient along the line $\partial u / \partial y = 0$. In a general flow field where these constraints are not met, the error can be reduced by decreasing the delay time Δt, but it cannot be made arbitrarily small, since Δt needs to be large enough for the resulting displacement of the tagged line to be measured with adequate accuracy. While keeping these issues in mind, it is sometimes possible to take advantage of an *a priori* knowledge of the flow field under investigation to design the experimental parameters such that the inherent error discussed here becomes minimal compared to other measurement errors. Representative examples of fluid flow measurements obtained with line tagging methods include studies of jets (Miles et al. 1989a,b; 1993; Noullez et al. 1997; Lempert et al. 2002; 2003), boundary layers (Hill and Klewicki 1996; Klewicki and Hill 2003), pulsatile flow through tubes (Ojha et al. 1989), particle-laden coaxial jets (Sadr and Klewicki 2005), buoyancy-induced flow in directional solidification (Wirtz et al. 1998; Lum 2001; Lum et al. 2001), and axial flow within concentrated vortex cores (Bohl 2002; Bohl and Koochesfahani 2004). MTV with line tagging has also found extensive use in microfluidic applications where the flow is primarily unidirectional (e.g. Paul et al. 1998; Mosier et al. 2002; Maynes and Webb 2002; Sinton et al. 2004; Lum 2005).

In order to unambiguously measure two components of the velocity in a plane, the luminescence intensity field from a tagged region must have spatial gradients in two, preferably orthogonal, directions. For single-point velocimetry, this can be achieved using a pair of crossing laser beams and measuring the displacement of the beam intersection; a grid of intersecting laser beams allows multi-point velocity measurements as illustrated in Figure 1. This tagging scheme, first suggested by D'Arco et al. (1982) and later improved upon and utilized by Falco and Chu (1987), is now commonly used.

The methods used to date for generating a grid of intersecting laser beams typically rely on standard optics (i.e. beam splitters, mirrors, spherical and cylindrical optics, and beam blockers). For example, the tagging pattern shown in Figure 1 is generated by manipulating the main beam of an excimer laser to increase its aspect ratio using a cylindrical lens, followed by splitting the outgoing laser sheet with a 50:50 beam splitter and redirection by mirrors, and then passing them through a pair of beam blockers (Gendrich et al. 1997). Spherical lenses are used as needed to control the spatial scaling of the entire grid pattern. The maximum density of grid intersections is limited by different factors depending on the type of molecular tracer that is used. In some cases the energy requirements to create the tag and detection sensitivity set the limit. Miles et al. (2000) have reported a single-intersection created with RELIEF, whereas Pitz et al. (2005) have recently achieved a 7×7 grid pattern with their HTV approach using OH (see Figure 13). When using phosphorescent tracers for MTV in both gas-phase and liquid-phase flows, the energy in each tagging beam is typically in the range 1–2 mJ or less per pulse and the maximum grid density has been limited not by the available laser energy but by the pixel density of the imaging detector arrays used (Gendrich et al.

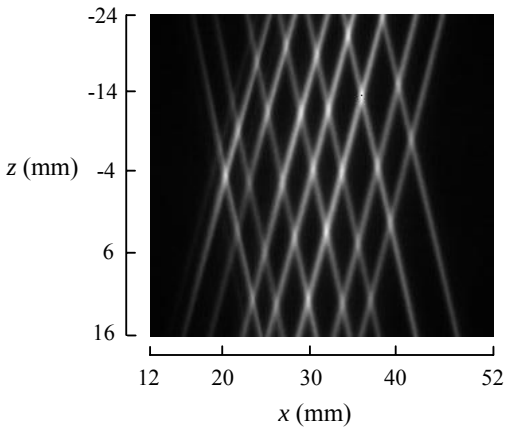

Fig. 13. A 7 × 7 grid of tagged OH lines in a supersonic flow (Mach number 2) over a cavity (Pitz et al. 2005).

1997; Cohn 1999; Stier and Koochesfahani 1999). For 640 pixel × 480 pixel detector arrays, tagging with a grid pattern in the range 30 × 30 has been achieved. Recent work with higher resolution detectors (1280 pixel × 1024 pixel array) tags the phosphorescent molecules in a water flow with about a 70 × 70 grid pattern (Hu and Koochesfahani 2006).

It is useful to note that tagging by a non-uniform laser illumination in the form of a grid is needed when the molecular tracer is present uniformly in the fluid. This method is only a special case of a more generalized approach to induce a spatially non-uniform luminescence intensity in a tagged region. For example, the non-uniform passive scalar field typical of most turbulent flows can sometimes be used as a natural source of luminescence non-uniformity without the need for grid illumination, or further enhancement of the effect of grid illumination. Examples of this type are discussed in Koochesfahani et al. (1996) and Gendrich et al. (1997).

3.2 Detection

The most common implementation of MTV uses a single detector; the initial (or reference) tagging pattern is recorded once, usually at the beginning of the experiment, and then the "delayed" images are acquired. This approach works well as long as the initial tagging pattern remains spatially invariant throughout the experiment. Otherwise, any variations in the initial tagging pattern (e.g. due to laser beam pointing instability, vibration of the optics, non-uniform tracer concentra-

tion, etc.) is misinterpreted as flow velocity fluctuations and reduces the measurement accuracy of the instantaneous velocity.

In order to minimize the potential problems just noted, Gendrich et al. (1997) have implemented a two-detector imaging system for their work with phosphorescent tracers. The MTV image pairs are acquired by a pair of CCD detectors that view the same region of interest in the flow through a beam splitter. Using a reference target, the two cameras are aligned to within one pixel, and the remaining residual displacement field between the two detectors is quantified to sub-pixel accuracy and accounted for in subsequent data processing (for details see Gendrich et al. 1997). Immediately after the pulsed laser fires to tag the molecules in the flow, the first detector records an initial image of the tagged regions. After a prescribed time delay, the second detector records a second image of the tagged regions displaced by the flow. Such a two-image system offers advantages over the typical single-image system in that no assumption needs to be made *a priori* about the intensity field in a tagged region and one can properly take into account the variations in the initial tagging pattern. Two-detector imaging has been used in many MTV studies, especially those based on phosphorescent tracers (e.g. Gendrich et al. 1997; Gendrich 1998; Cohn 1999; Cohn and Koochesfahani 1999; Goh 2001; Koochesfahani et al. 2000; Lum 2001; Lum et al. 2001; Bohl 2002; Koochesfahani and Bohl 2002; Sadr and Klewicki 2003a; Bohl and Koochesfahani 2004; Lum 2005).

The one- or two-detector scheme described above addresses conventional planar imaging for obtaining information on two components of the velocity vector over the viewed plane (or one velocity component in the case of line tagging). When stereo imaging is used to also obtain the out-of-plane velocity component (Krüger and Grünefeld 1999; Bohl et al. (2001), the number of needed detectors increases by a factor of two. With advances in detector technology, the two-detector MTV approach can now be accomplished with a single "dual-frame" camera that allows the acquisition of two images of the tagged regions with a programmable time delay between them (Bohl 2002; Hu and Koochesfahani 2006). This capability not only simplifies the implementation of conventional MTV imaging but also provides for a significant reduction of effort in aligning multiple cameras in stereo imaging (Bohl 2002).

3.3 Processing

A common method for finding the displacement of tagged lines or grids has been to locate the center of each line through various techniques (Lempert et al. 1995; Hill and Klewicki 1996; Bohl and Koochesfahani 2004). One approach is to use the best fit to an assumed laser line shape, for example, a Gaussian intensity distribution (e.g. Lempert et al. 1995). Another is to use a second-order curve fit following Gaussian smoothing (Hill and Klewicki 1996). Hill and Klewicki (1996) report the rms accuracy in determining the displacement of a tagged line to be 0.35 pixel. The performance of these methods for finding line centers tend to suffer when the intensity distribution of the tagged regions cannot be assumed in ad-

vance, for example, due to non-uniform tracer distribution, difficulties associated with laser beam transmission through a flowing medium, photobleaching effects, etc. Sadr and Klewicki (2003) have recently explored a spline-based method and report an improvement in sub-pixel accuracy by about a factor of three.

Another approach for finding the displacement of tagged regions is based on a direct digital spatial correlation technique, and offers certain advantages over the traditional line-center methods. In particular, it is a more general scheme that is independent of the specific intensity distribution within a tagged region and can accommodate arbitrary tagging patterns including those due to non-uniform scalar mixing fields. The details of this approach and its performance are described in Gendrich and Koochesfahani (1996). A small window, referred to as the source window, is selected from a tagged region in the earlier undelayed image, and it is spatially correlated with a larger roam window in the second delayed image. A well-defined correlation peak occurs at the location corresponding to the displacement of the tagged region by the flow; the displacement peak is located to sub-pixel accuracy using a multi-dimensional polynomial fit (see example in Figure 14). This approach is similar to that used in DPIV processing of particle image pairs and, because of the averaging process inherent in the correlation procedure, it is more robust to the presence of noise and typically more accurate than line-center methods. Based on both experiments and an extensive statistical study, it has been found that the displacement of the tagged regions can be typically determined with a 95% confidence limit of 0.1 sub-pixel accuracy (i.e. 95% of the displacement measurements are accurate to better than 0.1 pixel). This corresponds to an rms accuracy of 0.05 pixel, assuming a Gaussian distribution for error. For high values of image signal to noise ratio, the 95% confidence level can be as low as 0.015 pixel (0.0075 pixel rms). An example of the application of this

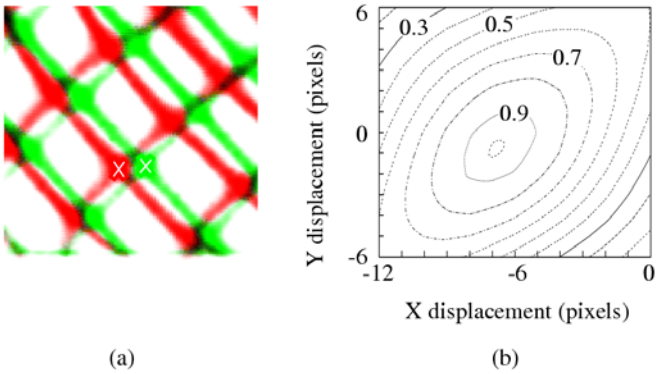

Fig. 14. (a) Superposed experimental MTV image pair: green lines are the grid at $t = 0$, red lines are the grid after $\Delta t = 6$ ms delay. (b) Correlation coefficient contours for the indicated intersection in (a) (Koochesfahani et al. 1996).

procedure is provided in Figure 1; the velocity vectors shown in this figure are "raw" and have not been filtered or smoothed.

The spatial correlation method described above has also been applied to processing line tagging images in an investigation of flows in microchannels (Maynes and Webb 2002; Lum 2005). In this case, a one-dimensional correlation procedure is used and accuracies similar to Gendrich and Koochesfahani (1996) are obtained. A modified version of the two-dimensional spatial correlation method of Gendrich and Koochesfahani (1996) has been introduced by Zheng and Klewicki (2000) where the sub-pixel accuracy is determined not based on the original multi-dimensional polynomial fit but using two decoupled polynomials. This approach offers a faster computational algorithm at the expense of reduced accuracy. Other processing methods such as the image correlation velocimetry approach of Tokumaru and Dimotakis (1995) have also been applied to MTV image pairs (see Pitz et al. 2000).

MTV velocity data are obtained originally on an irregularly spaced measurement grid. In order to take advantage of standard data display and processing techniques, the data need to be remapped onto a regular grid with uniform spacing. One method that has been used for this purpose is based on a least-squares-fit to low order polynomials. The details of the procedure and its performance characteristics are given by Cohn and Koochesfahani (2000). The velocity field on a regular grid is then used to compute the vorticity field in the same manner as in DPIV data. Typically a finite difference approach, for example 2^{nd} order central difference, is utilized (see e.g. Gendrich et al. 1997; Cohn and Koochesfahani 2000). The accuracy of the measured vorticity depends on the accuracy in the velocity measurement and the data grid spacing. Vorticity measurement accuracies in the range $1 - 2\ s^{-1}$ (95% confidence limit) have been reported (Cohn 1999; Cohn and Koochesfahani 1999).

An example of MTV data obtained by the procedures described above is given in Figure 15. This example shows the instantaneous whole-field measurement of two components of the velocity vector over a plane in a study of unsteady boundary-layer separation caused by the interaction of a vortex ring impinging on a solid wall. This interaction generates an unsteady adverse pressure gradient on the wall, which results in boundary layer separation and the formation of a secondary vortex. An LIF visualization of this flow right after the formation of the secondary vortex is depicted in Figure 15(a) (only the right half of the flow is included). Figure 15(b) shows the corresponding instantaneous MTV velocity data (1 mm grid spacing with the first grid 0.5 mm away from the wall) and the computed vorticity field. These data have sufficient resolution to study the behavior of the unsteady boundary layer on the wall and the progression of the boundary layer separation process (Gendrich et al. 1997).

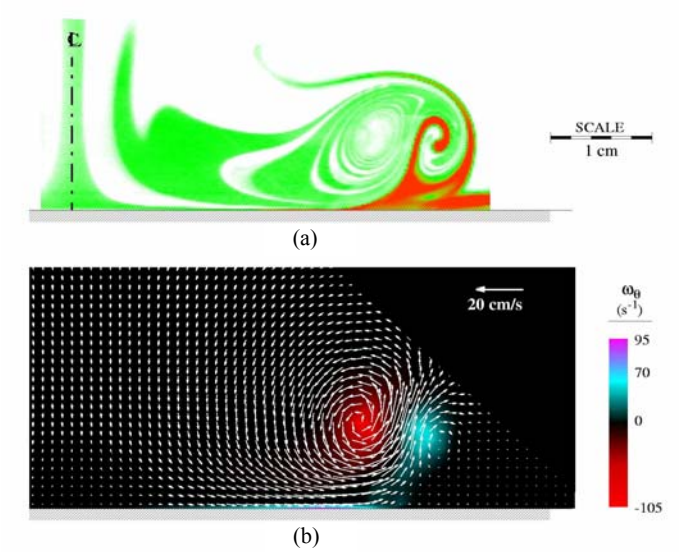

Fig. 15. (a) LIF image of the right-half of a downward moving vortex ring impinging on a solid wall. The ring and wall-layer fluids are marked by green- and red-emitting laser dyes, respectively. (b) Velocity and vorticity fields measured using MTV (Koochesfahani et al. 1996)

4. Examples of MTV Measurements

The references cited in this work present the development and application of molecular tagging velocimetry in flows over a wide range of speeds, from liquid-phase microfluidic flows with speeds that are measured in μm/s to gas-phase flows at supersonic speeds. The scope of the measurements covers a range from the instantaneous profile of one component of velocity vector along a tagged line to whole-field three-component velocity data over a plane obtained with stereo imaging. Some of the flows that have been successfully investigated include pulsatile flow in tubes, pressure- and electroosmotically-driven microfluidics, internal circulation in droplets, unsteady boundary layer separation, vortex flows and mixing enhancement, convective flows in directional solidification, flows during intake and compression inside motored IC engines, flows in engine testing facilities, high-temperature reacting flows, free and wall-bounded turbulent flows, and highly three-dimensional vortex flows with strong out-of-plane motions where the primary flow direction is normal to the tagged plane.

In this section we provide several examples to highlight some of the measurement capabilities that have been achieved with molecular tagging velocimetry based on phosphorescent tracers (MTV mechanism D). These examples consider

only velocimetry applications. The unique properties of some molecular tracers have led to novel methods for studying scalar mixing in turbulent flows using caged fluorescent dyes (Guilkey et al. 1996; Hansen et al. 2000) and high sensitivity temperature measurements with phosphorescent supramolecules (Hu et al. 2006). In addition, MTV has been extended to multi-variable mapping such as simultaneous velocity-concentration (Koochesfahani et al. 2000) and velocity-temperature (Thomson & Maynes 2001; Hu and Koochesfahani 2003; 2006).

4.1 Boundary-Layer Resolved Measurements of Leading-Edge Separation on a Pitching Airfoil

When an airfoil dynamically pitches to high angles of attack the viscous boundary layer near the leading edge eventually separates and eventually causes catastrophic events such as dynamic stall. The evolution of the flow within the boundary layer at the onset of separation has been captured with molecular tagging velocimetry (Gendrich 1998), providing the first detailed map of the events that occur within the boundary layer near the surface of a pitching airfoil. Results shown in Figure 16 are from measurements carried out in a 60 cm × 60 cm water tunnel using a 12-cm chord NACA-0012 airfoil pitching at a constant rate (non-dimensional pitch rate = 0.1) from 0 to 60 degrees angle of attack. The chord Reynolds number is about 12,000. Since the range of spatial scales in this problem is too large to be captured in a single field of view, these measurements are carried out over multi-

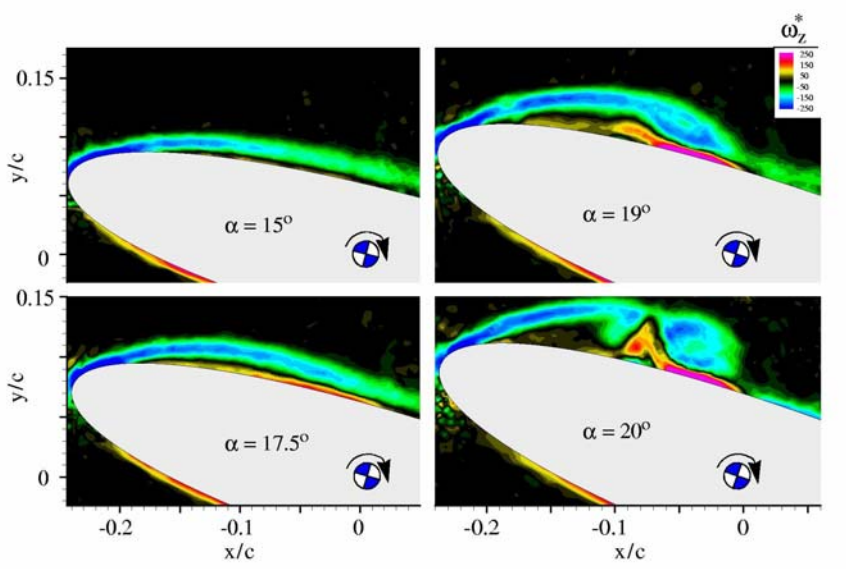

Fig. 16. Evolution of the vorticity field at the onset of leading-edge separation on an airfoil pitching to high angles of attack (Gendrich 1998).

ple fields of view with decreasing size. Repeatability of this flow allows the data to be compiled into a single finely-resolved data set for each 0.25 degree change in angle of attack.

The non-dimensional vorticity field computed from this data set is shown in Figure 16 at four angles of attack near the onset of leading-edge separation. These results illustrate the ability of MTV in imaging fluid flows near walls. Among the details that are resolved in these measurements are the occurrence of a thin reversed flow region near the airfoil surface, and the eruption of the boundary layer vorticity away from the wall in a highly localized manner in both time and space. Complementary two-dimensional Navier-Stokes computations have also been carried out at the flow conditions of these experiments. A conclusion from these experimental data is that the process of boundary layer separation occurs over a shorter time scale, and is more eruptive, than that captured by the computations.

4.2 Measurement of Buoyancy-Driven Convective Flow during Uni-Directional Solidification

Solidifying a binary alloy under off-eutectic conditions is often accompanied by convection in the melt. The convection mechanisms caused by solutal and thermal forces for such conditions can produce inhomogeneities and imperfections such as solute-rich channels in the final fully solidified ingot casting. While the convective phenomena involved in the formation of these imperfections are not completely understood, it is generally accepted that they are best described in terms of complex dynamic fields and that most experimental methods applied to date are poorly suited to measure these fields. One means of learning more about these phenomena has been the use of transparent analogs of metallic alloys. One such analog is the binary aqueous ammonium chloride (NH_4Cl-H_2O) system. Some of the complex features of convective phenomena associated with solidification in the aqueous ammonium chloride include: the vertical growth of a solid/liquid interface with concurrent early development of numerous fine structures of salt fingers followed by the appearance of a small number of plumes ejecting fluid jets from channels in the mushy zone of the growing dendritic crystal mass. These features are illustrated in the shadowgraph images in Figure 17 (Lum 2001; Lum et al. 2001).

Measurement of this flow field by particle-based techniques can be problematic since the presence of particles could interfere with the solidification process and create unwanted nucleation sites. In addition, the mushy zone acts as a very fine-scale porous medium and traps the particles that are contained within the liquid above. As a result, the fluid within the plume is often devoid of particles. The MTV approach using phosphorescent supramolecules have been used to measure the velocity field within and around the plumes (Lum 2001; Lum et al. 2001). The portion of the flow near the bottom of the plume is mostly unidirectional (vertically upward flow) and single line tagging is sufficient to map the velocity profile within the plume. Farther up, however, two-component velocity maps are obtained using molecular tagging by an intersecting grid of laser lines. A unique as-

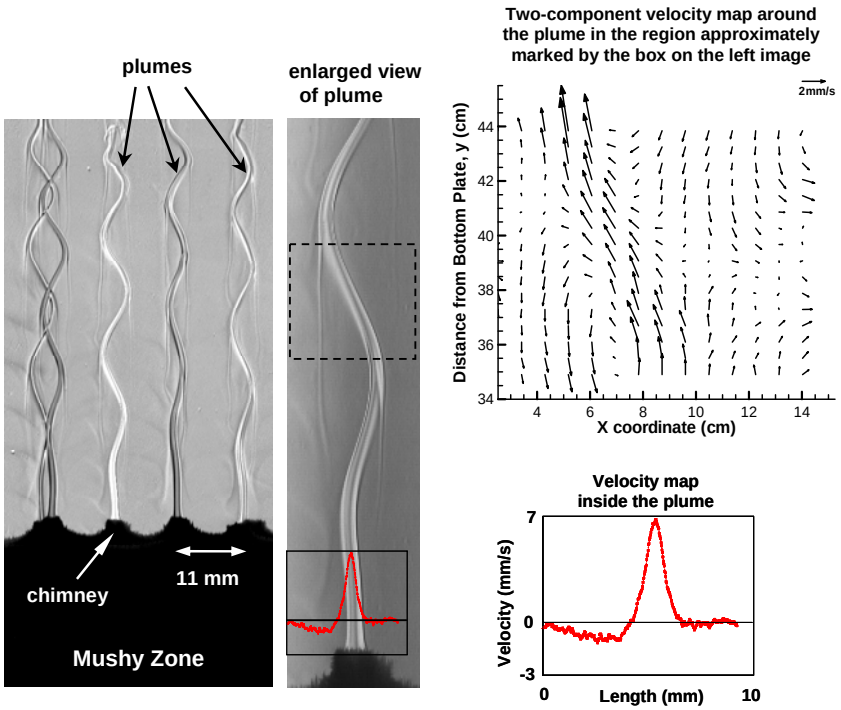

Fig. 17. Shadowgraph image of organized plumes above an advancing solidification front and the velocity fields measured by MTV (Lum 2001). The velocity profile at bottom of plume is measured using line tagging.

pect of these measurements is that the time delay between tagging and interrogation needs to be long due to the slow flow speeds involved. The 60 ms delay time used in these measurements is about a factor of 12 longer than the phosphorescence lifetime (i.e. 1/*e* point) of the tracer used, resulting in a significant reduction of phosphorescence emission intensity and necessitating the use of an intensified camera for detection.

Figure 17 shows the measured instantaneous velocity profile across a single plume as it exits the chimney, and the velocity map around the plume farther up. The upward jet-like velocity field within the plume is captured along with a non-symmetric downward flow around the plume. Note the peak velocity is only 7 mm/s and the width of the plume is about 2 mm.

4.3 Measurements in a "Steady Flow Rig" Model of an IC Engine

The steady flow rig configuration is commonly used in the internal combustion (IC) engine research community to study the fundamentals of the intake flow. The particular geometry used here consists of a quartz cylinder of radius R_o = 41 mm, placed axisymmetrically around a nozzle with a valve body placed axisymmetrically inside the jet nozzle. In this case the flow exiting through the valve opening, which simulates the intake flow into an IC engine geometry, is in the form of an annular jet. In this study, the valve opening (valve lift) is set at L = 9 mm and the maximum intake speed is about 10 m/s. The instantaneous accelerations in the shear layer at the interface between the intake jet and adjacent fluid can be as high as 5000 g, making it difficult to rely on the results of particle-based techniques. The details of this work can be found in Stier & Koochesfahani (1999).

Figure 18 shows a 3 cm × 3 cm field of view in the nitrogen/biacetyl flow being investigated and the regions tagged by a grid pattern generated from an excimer laser (λ = 308 nm, 20 ns pulse). Part of the valve body and the left wall of the cylinder are visible in the picture. The maximum flow speed in the annular jet entering the cylinder is about 10 m/s. Also shown is an example of the later image of the tagged regions after a 50 μs delay. For this time delay, the maximum displacement of tagged regions is about 8 pixels (~ 500 μm). Image pairs such as those in Figure 18 are used to determine the instantaneous radial and axial velocity components in this flow field. An example of the instantaneous velocity field and the structure of the intake flow in this geometry are shown in Figure 19 along with the average velocity field based on 320 realizations. The instantaneous flow map shows a highly unsteady intake annular jet, which has an undulating appearance with opposite sign large scale vortical structures on its two sides. The mean flow

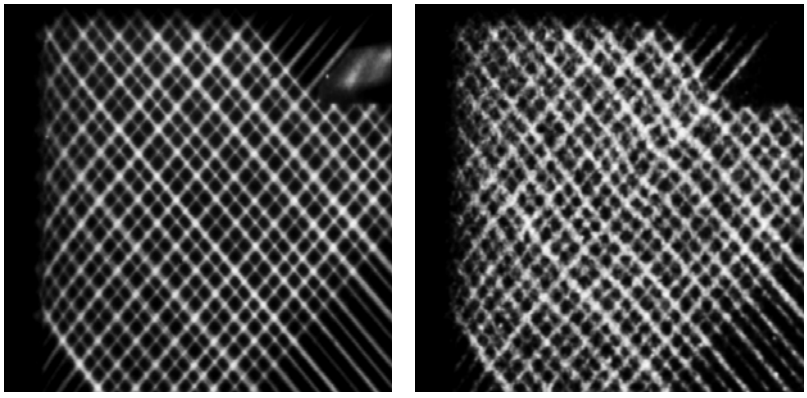

Tagged regions right after the laser pulse

Tagged regions 50 μs later; 3 cm × 3 cm field of view

Fig. 18. Example of the tagging pattern for the gas flow into the steady flow rig (Stier and Koochesfahani 1999). Images are acquired by a gated image-intensified camera.

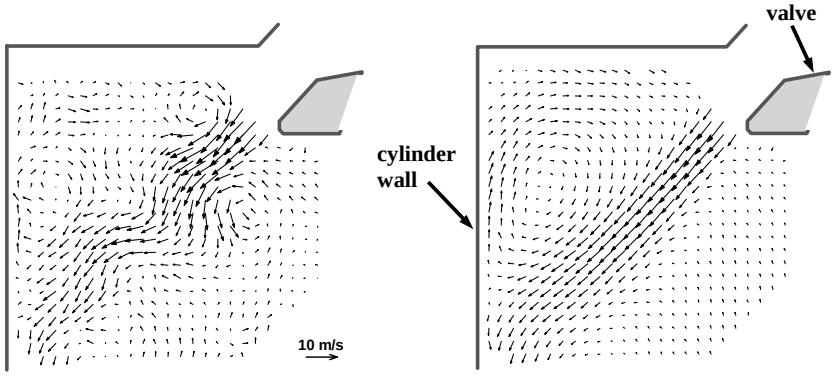

The instantaneous velocity field derived from the image pair in Figure 18 using a spatial correlation procedure.

Time-averaged velocity field based on 320 instantaneous realizations.

Fig. 19. Intake flow into a steady flow rig model of IC engine measured with MTV using nitrogen seeded with biacetyl (Stier and Koochesfahani 1999).

map indicates a large scale region of recirculation in the upper left corner of the engine cylinder, a feature typical of an IC engine flow field. These data have also been used to derive other properties of the flow such as the instantaneous and average vorticity fields and velocity fluctuations (Stier and Koochesfahani 1999).

4.4 Velocity Field during Late Compression in a Motored IC Engine

One of the main obstacles in optimizing combustion in gasoline-fueled internal combustion engines is the large cycle-to-cycle variation in in-cylinder flow and mixing characteristics. Cycle-to-cycle variability puts constraints on the lean limits of combustion. In this study velocity field data are obtained using MTV during late compression of an internal combustion engine, the most critical time of the four-stroke cycle. Such data are highly sought since the state of the flow just before the firing of the spark plug directly influences the subsequent combustion and emission production.

The measurements are conducted in an optically accessible motored research engine shown in Figure 20. The cylinder is made from quartz and the flat-head piston face is modified for optical access through a quartz window. A typical MTV grid generated within the engine cylinder is also shown in Figure 20. Measurements are made at late compression at a crank angle of 270 Crank Angle Degree (CAD), as the piston approaches the Top Dead Center (TDC) of the engine, with the engine running at 600 RPM. For the conditions described here, and

the engine compression ratio of nearly 10, the gas temperature can reach a value as high as 600K. The measurements consist of 500 independent realizations of the velocity map at the same crack angle (270 CAD) at the mid-tumble-plane. The position of the imaged plane over which the velocity maps are obtained is given in Figure 21. The details of this work can be found in Goh (2001).

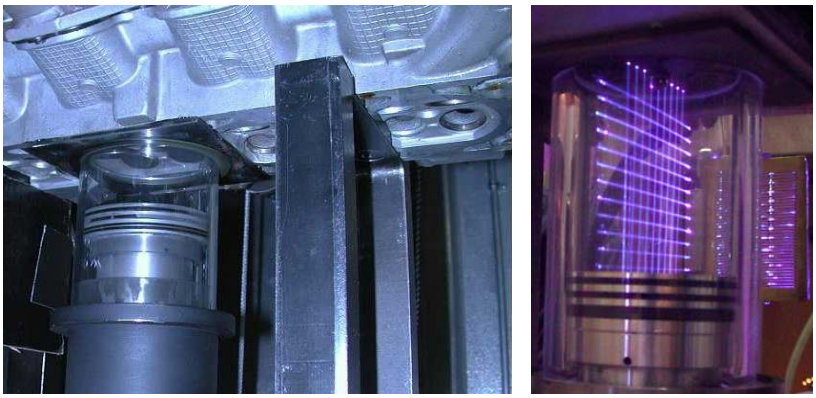

Optically accessible Ford 4-valve, 4.6L engine Sample MTV grid

Fig. 20. The optically accessible research engine and a typical MTV grid in the nitrogen/biacetyl flow within the engine cylinder (Koochesfahani et al. 2004).

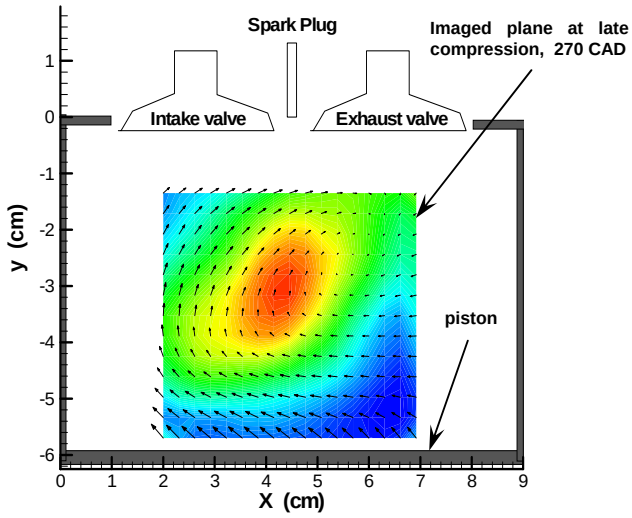

Fig. 21. The position of the imaged plane at 270 CAD (Goh 2001).

Two samples of the instantaneous velocity field, for two different engine cycles, are shown in Figure 22. It is clear the flow pattern is significantly different between these two realizations, an indication of the large cycle-to-cycle variability of the flow. The maps of the ensemble-averaged velocity field and the rms fluctuation of the horizontal velocity component are computed from 500 such realizations, see Figure 23. As expected for a flow with large cycle-to-cycle variation, the mean velocity field has little resemblance to the instantaneous field; the local fluctuation level can be higher than the mean by several hundred percent. The data shown in Figures 22 and 23 are the first cycle-resolved velocity measurements that use molecular tracers rather than particles to determine flow velocities in a piston-engine assembly. Such measurements have been used to advance the understanding and quantification of cycle-to-cycle variability in an internal combustion engine, and finding methods for reducing it (Goh 2001).

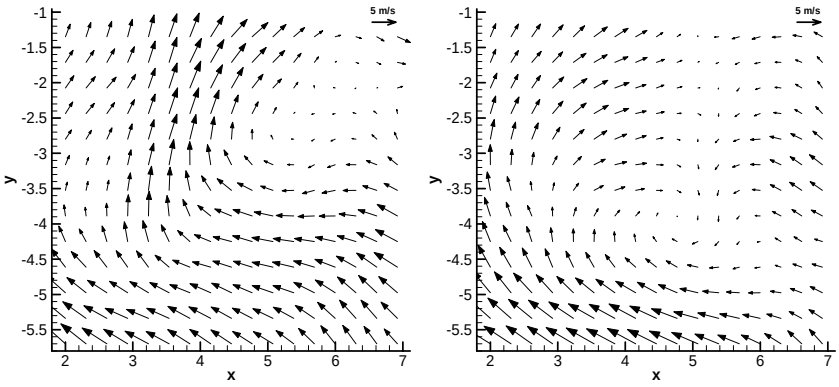

Fig. 22. Two instantaneous realizations at 270 CAD showing the large cycle-to-cycle variability of the flow field (Goh 2001).

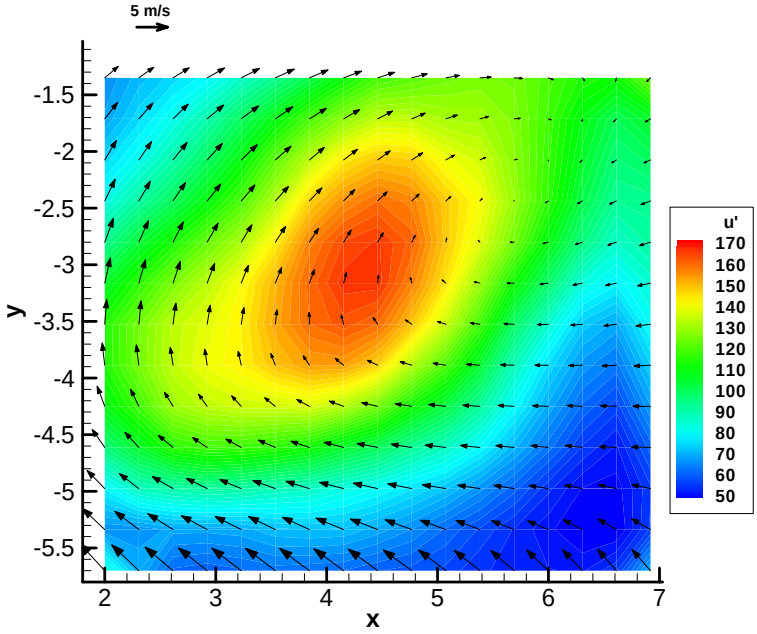

Fig. 23. Maps of the ensemble-averaged velocity field and the rms fluctuation of the horizontal component of velocity u′ (in cm/s) (Goh 2001). Colors denote rms fluctuation level.

6. Summary and Conclusions

Molecular tagging velocimetry has seen significant advances as a result of improvements in laser and detector technologies, imaging techniques, data analysis methods, and chemical design and synthesis of novel molecular structures. These advances are expected to continue. The MTV approach has continuously evolved and its use is steadily increasing in both fundamental flow studies and applied engineering measurements.

7. References

Balzani V. and Carassiti V. (1970) Photochemistry of Coordination Compounds, London: Academic

Balzani, V., Moggi, L., Manfrin, M. F., and Bolletta, F. (1975) Quenching and sensitization processes of coordination compounds. *Coord Chem Rev*, vol. 15, 321-433.

Balzani, V., Bolletta, F., and Scandola, F. (1980) Vertical and "nonvertical" energy transfer processes - a general classical treatment, *J. Am. Chem. Soc*., vol. 102, 2152-2163.

Balzani, V, and Scandola, F. (1991) Supramolecular Photochemistry, Chichester: Ellis-Horwood

Barker, P., Thomas, A., Rubinsztein-Dunlop, H., and Ljungberg, P. (1995) Velocity measurements by flow tagging employing laser-enhanced ionisation and laser induced fluorescence, *Spectrochim Acta B*, vol. 50, 1301-1310.

Biage, M., Harris, S. R., Lempert, W. R., and Smits, A. J. (1996) Quantitative velocity measurements in turbulent Taylor-Couette flow by PHANTOMM flow tagging, *Proceedings of the Eighth International Symposium on Applications of Laser Techniques to Fluid Mechanics*, Lisbon, Portugal, July 8-11, 1996, 15.4.1-15.4.8.

Boedecker, L. R. (1989) Velocity measurements by H_2O photolysis and laser-induced fluorescence of OH, *Optics Letters*, vol. 14, no. 10, 473-475.

Bohl, D., and Koochesfahani, M., and Olson, B. (2001) Development of stereoscopic Molecular Tagging Velocimetry," *Exp. Fluids*, vol. 30, 302-308.

Bohl, D. G. (2002) Experimental Study of the 2-D and 3-D Structure of a Concentrated Line Vortex Array, PhD thesis, Michigan State University, East Lansing, MI, USA.

Bohl, D. G. and Koochesfahani, M. M. (2004) MTV measurements of axial flow in a concentrated vortex core, *Phys. Fluids*, vol. 16, no. 11, 4185-4191.

Bünzli, J-CG., (1988) Luminescent probes, In *Lanthanide Probes in Life, Chemical and Earth Sciences* (eds. Bünzli, J.-G.C., Choppin, G.R.) pp. 219-293, Amsterdam: Elsevier

Chu, C. C. and Liao, Y. Y. (1992) A quantitative study of the flow around an impulsively started circular cylinder, *Exp. Fluids*, vol. 13, 137-146.

Chu, C. C., Wang, C. T., and Hsieh, C. H. (1993) An experimental investigation of vortex motions near surfaces, *Phys. Fluids A.*, vol. 5, no. 3, 662-676.

Chu, C. C., Wang, C. T., Chang, C. C., Chang, R. Y. and Chang, W. T. (1995) Head-on collision of two coaxial vortex rings: experimental and computation, *J. Fluid Mech*., vol. 296, 39-71.

Cohn, R. K. (1999) Effect of forcing on the vorticity field in a confined wake, PhD thesis, Michigan State University, East Lansing, MI, USA.

Cohn, R. K. and Koochesfahani, M. M. (1999) Vorticity field evolution in a forced wake, *Proceedings of the 1st International Symposium on Turbulence and Shear Flow Phenomena*, Santa Barbara, CA, Sep. 12-15, 1999, Eds. Banerjee, S., and Eaton, J. K., pp. 901-906.

Cohn, R. K., and Koochesfahani, M. M. (2000) The accuracy of remapping irregularly spaced velocity data onto a regular grid and the computation of vorticity, *Exp. Fluids*, vol. 29, S61-S69.

Couch, G. G., Johnston, K. W., and Ohja, M. (1996) Full-field flow visualization and velocity measurement with a photochromic grid method, *Meas. Sci. Technol*., vol. 7, no. 9, 1238-1246.

Crimaldi, J. P. (1997) The effect of photobleaching and velocity fluctuations on single-point LIF measurements, *Exp Fluids*, vol. 23, 325-330.

Dam, N. J., Klein-Douwel, RJH, Sijtsema, N.M., and ter Meulen, J.J. (2001) Nitric oxide flow tagging in unseeded air, *Opt Lett*., vol. 26, 36-38

D'Arco, A., Charmet, J. C., and Cloitre, M. (1982) Nouvelle technique de marquage d'ecoulement par utilisation de molecules photochromes, *Revue Phys. Appl*., vol. 17, 89-93.

Endicott, J.F. (1988) Manipulation of superexchange couplings, *Acc. Chem. Res*., vol. 21, 59-66.

Exton, R.J. and Hillard, M. E. (1986) Raman Doppler velocimetry - A unified approach for measuring molecular-flow velocity, temperature, and pressure, *Applied Optics*, vol. 25, 14-21

Falco, R. E. and Chu, C. C. (1987) Measurement of two-dimensional fluid dynamic quantities using a photochromic grid tracing technique, *SPIE,* vol. 814, 706-710.

Falco, R. E. and Nocera, D. G. (1993) Quantitative multipoint measurements and visualization of dense solid-liquid flows using laser induced photochemical anemometry (LIPA) *Particulate Two-Phase Flow*, ed. M. C. Rocco (London: Butterworth-Heinemann), 59-126

Feast, M. W. (1948) Emission Schumann-Runge O_2 bands, *Nature*, vol. 162, 214-215

Forster, L.S. (1975) Photophysical processes - energy levels and spectra. In: Concepts of Inorganic Photochemistry (eds. Adamson A.W.; Fleischauer P.D.) pp. 1-35, New York: Wiley-Interscience

Frantisak, F., Palade de Iribarne, A., Smith, J. W., and Hummel, R.L. (1969) Nondisturbing tracer technique for quantitative measurements in turbulent flows. *Ind Eng Chem Fundam*, vol.8, 160-167

Freed, K.F. (1978) Radiationless transitions in molecules, *Acc Chem Res*, vol. 11, 74-80

Frey, R., Lukasik, J., and Ducuing, J. (1972) Tunable Raman excitation and vibrational relaxation in diatomic molecules, *Chemical Physics Letters*, vol. 14, no. 4, 514-517.

Gendrich, C. P. and Koochesfahani, M. M. (1996) A spatial correlation technique for estimating velocity fields using Molecular Tagging Velocimetry (MTV), *Exp. Fluids*, vol. 22, no. 1, 67-77.

Gendrich, C. P., Koochesfahani, M. M. and Nocera, D. G. (1997) Molecular tagging velocimetry and other novel applications of a new phosphorescent supramolecule, *Exp. Fluids*, vol. 23, no. 5, 361-372.

Gendrich, C. P., Bohl, D. G., and Koochesfahani, M. M. (1997) Whole-field measurements of unsteady separation in a vortex ring/wall interaction, AIAA paper AIAA-97-1780.

Gendrich, C. P. (1998) Dynamic stall of rapidly pitching airfoils: MTV experiments and Navier-Stokes simulations, PhD thesis, Michigan State University, East Lansing, MI, USA.

Goh, A. C. H. (2001) Active flow control for maximizing performance of spark-ignited stratified charge engines, MS thesis, Michigan State University, East Lansing, MI, USA.

Goss, L., Chen, T., Trump, D., Sarka, B., and Nejad, A. (1991) Flow tagging velocimetry using UV- photodissociation of water vapor, AIAA paper AIAA-91-0355.

Goss, L., Chen, T., Schommer, D., and Nejad, A. (1992) Laser diagnostics for velocity measurements in supersonic combusting environments, AIAA paper AIAA-92-0008.

Guilkey, J. E., Gee, K. R., McMurtry, P. A., and Klewicki, J. C. (1996) Use of caged fluorescent dyes for the study of turbulent passive scalar mixing, *Exp. Fluids*, vol. 21, 237-242.

Hansen, L., Guilkey, J. E., McMurtry, P. A., and Klewicki, J. C. (2000) The use of photoactivatable fluorophores in the study of turbulent pipe mixing: effects of inlet geometry, *Meas. Sci. Technol*., vol. 11, no. 9, 1235-1250.

Harris, S. R., Lempert, W. R., Hersh, L., Burcham, C. L., Saville, A., Miles, R. B., Gee, K., and Haughland, R. P. (1996a) Quantitative measurements on internal circulation in droplets using flow tagging velocimetry, *AIAA J*., vol. 34, no. 3, 449-454.

Harris, S. R., Miles, R. B., and Lempert, W. R. (1996b) Observations of fluid flow produced in a closed cylinder by a rotating lid using the PHANTOMM (Photo-Activated Non Intrusive Tracking of Molecular Motion) flow tagging technique, *Proceedings of the Eighth International Symposium on Applications of Laser Techniques to Fluid Mechanics*, Lisbon, Portugal, July 8-11, 1996, 15.3.1-15.3.9.

Harris, S. R. (1999) Quantitative measurements in a lid driven, cylindrical cavity using the PHANTOMM flow tagging technique, PhD thesis, Princeton University, Princeton, NJ, USA.

Hartmann, W. K., Gray, M. H. B., Ponce, A., and Nocera, D. G. (1996) Substrate induced phosphorescence from cyclodextrin • lumophore host-guest complexes, *Inorg. Chim. Acta*, vol. 243, 239-248.

Hascher, H. G., Novak, M., Lee, K., Schock, H., Rezaei, H., and Koochesfahani, M. M. (1998) An evaluation of IC-engine flow with the use of modern in-cylinder measuring techniques, AIAA paper AIAA-98-3455.

Herzberg, G. (1950) Molecular Spectra and Molecular Structure: Spectra of Diatomic Molecules - Second Edition. New York: van Nostrand.

Hill, R. B. and Klewicki, J. C. (1996) Data reduction methods for flow tagging velocity measurements, *Exp. Fluids*, vol. 20, no. 3, 142-152.

Hiller, B., Booman, R.A., Hassa, C., and Hanson, R.K. (1984) Velocity visualization in gas flows using laser-induced phosphorescence of biacetyl, *Rev. Sci. Inst*., vol. 55, 1964-1967.

Hilbert, H. S. and Falco, R. E. (1991) Measurements of flows during scavenging in a two-stroke engine, SAE Technical Paper 910671.

Hummel, R.L. (1976) Nondisturbing flow measurement using a photochromic tracer technique. High Speed Photography *SPIE*, vol. 97, 302-307.

Horrocks, W. and Albin, M. (1983) Lanthanide ion luminescence in coordination chemistry and biochemistry, *Prog. Inorg. Chem*., vol. 30, 1-104.

Hu, H. and Koochesfahani, M. M. (2003) A novel technique for quantitative temperature mapping in liquid by measuring the lifetime of laser induced phosphorescence, *Journal of Visualization*, vol. 6, no. 2, 143-153.

Hu, H., Lum, C., and Koochesfahani, M. M. (2006) Molecular tagging thermometry with adjustable temperature sensitivity," *Exp. Fluids*, vol. 40, 753-763.

Hu, H. and Koochesfahani, M. M. (2006) Molecular tagging velocimetry and thermometry technique and its application to the wake of a heated cylinder, *Meas. Sci. Technol*., vol. 17, 1269-1281.

Jortner, J., Rice, S. A., and Hochstrasser, R. M. (1969) Radiationless transitions in photochemistry, *Adv Photochem*, vol. 7, 149-309.

Klewicki, J. C. and Hill, R. B. (2003) Laminar boundary layer response to rotation of a finite diameter surface patch, *Phys Fluids*, vol. 15, no. 1, 101-111.

Koochesfahani, M. M. (1984) Experiments on turbulent mixing and chemical reactions in a liquid mixing layer. PhD thesis, California Institute of Technology, Pasadena, CA, USA.

Koochesfahani, M. M., Cohn, R. K., Gendrich, C. P. and Nocera, D. G. (1996) Molecular tagging diagnostics for the study of kinematics and mixing in liquid phase flows, *Proceedings of the Eighth International Symposium on Applications of Laser Techniques to Fluids Mechanics*, July 8 - 11, 1996, Lisbon, Portugal, vol. I, 1.2.1-1.2.12; Also in *Developments in Laser Techniques and Fluid Mechanics*, Chapter 2, section 1, p. 125, Eds. Adrian, Durao, Durst, Maeda, and Whitelaw; Springer-Verlag, Berlin, 1997.

Koochesfahani, M. M. (1999) Molecular Tagging Velocimetry (MTV): Progress and Applications, AIAA paper AIAA-1999-3786.

Koochesfahani, M. M. (Ed) (2000) Special Feature: Molecular Tagging Velocimetry, *Meas. Sci. Technol*., vol. 11, no. 9, 1235-1300.

Koochesfahani, M., Cohn, R, and MacKinnon, C. (2000) Simultaneous whole-field measurements of velocity and concentration fields using combined MTV and LIF, *Meas. Sci. Technol*., vol. 11, no. 9, 1289- 1300.

Koochesfahani, M. M. and Bohl, D. (2002) Molecular tagging visualization and velocimetry of the flow at the trailing edge of an oscillating airfoil, *Proceedings of the 10th International Symposium on Flow Visualization*, Kyoto, Japan, Paper No. F0453.

Koochesfahani, M. M., Goh, A. C., and Schock, H. J. (2004) Molecular Tagging Velocimetry (MTV) and its automotive applications, In *The Aerodynamics of Heavy Vehicles: Trucks, Busses, and Trains*, Lecture Notes in Applied and Computational Mechanics, vol. 19, 143-155, eds. R. McCallen, F. Browand, and J. Ross (Springer-Verlag).

Krüger, S. and Grünefeld, G. (1999) Stereoscopic flow-tagging velocimetry, *Appl. Phys. B*, vol. 69, 509-512.

Krüger, S. and Grünefeld, G. (2000) Gas-phase velocity field measurements in dense sprays by laser-based flow tagging, *Appl. Phys. B*, vol. 70, 463-466.

Lempert, W. R., Magee, K., Ronney, P., Gee, K. R., and Haughland, R. P. (1995) Flow tagging velocimetry in incompressible flow using photo-activated nonintrusive tracking of molecular motion (PHANTOMM), *Exp. Fluids*, vol. 18, 249-257.

Lempert, W. R. and Harris, S. R. (2000a) Molecular Tagging Velocimetry, *Flow Visualization – Techniques and Examples*, ed. A. J. Smits and T. T. Lim (London: Imperial College Press, London) 73-92.

Lempert, W. R. and Harris, S. R. (2000b) Flow tagging velocimetry using caged dye photo-activated fluorophores, *Meas. Sci. Technol*., vol. 11, no. 9, 1251-1258.

Lempert, W. R., Jiang, N., Sethuram, S., and Samimy, M. (2002) Molecular tagging velocimetry measurements in supersonic microjets, *AIAA J*., vol. 40, 1065-1070.

Lempert, W. R., Boehm, M., Jiang, N., Gimelshein, S., and levin, D. (2003) Comparison of molecular tagging velocimetry data and direct simulation Monte Carlo simulations in supersonic micro jet flows, *Exp Fluids*, vol. 34, 403-411.

Lin, S.H. (ed.) (1980) Radiationless Transitions. New York: Academic Press.

Liu, J.B., Pan, Q., Liu, C.S. and Shi, J.R. (1988) Principles of flow field diagnostics by laser induced biacetyl phosphorescence, *Exp. Fluids*, vol. 6, 505-513.

Lowry, H.S. (1987) Velocity measurements using the laser-induced phosphorescence of biacetyl, AIAA paper AIAA-87-1529.

Long, D.A. (1977) Raman Spectroscopy - Chap 8. New York: McGraw-Hill

Lu, L. J. and Smith, C. R. (1985) Image processing of hydrogen bubble visualization for determination of turbulence statistics and bursting characteristics, *Exp. Fluids*, vol. 3, 349-356.

Lum, C., Koochesfahani, M. M., and McGrath, J. J. (2001) Measurements of the velocity field with MTV during the solidification of an alloy analog with mushy region, ASME/IMECE2001 Paper HTD-24222.

Lum, C. (2001) Velocity field measurement for a uni-directional solidification of an ammonium chloride (NH_4Cl) solution using molecular tagging velocimetry (MTV), MS thesis, Michigan State University, East Lansing, MI., USA.

Lum, C. (2005) An experimental study of pressure- and electroosmotically-driven flows in microchannels with surface modifications, PhD thesis, Michigan State University, East Lansing, MI, USA.

Maynes, D. and Webb, A. R. (2002) Velocity profile characterization in sub-millimeter diameter tubes using molecular tagging velocimetry, *Exp. Fluids*, vol. 32, 3-15

McCray, J. A. and Trentham, D. R. (1989) Properties and uses of photoreactive caged compounds, *Ann. Rev. Biophys Chem*, vol. 18, 239-270

McKenzie, R. L. (1993) Progress in laser spectroscopic techniques for aerodynamic measurements: an overview, *AIAA J.*, vol. 31: 465-477.

Merzbacher, E. (1970) Quantum Mechanics, New York: Wiley

Meijer, G., ter Meulen, J. J., Andresen, P., and Bath, A. (1986) Sensitive quantum state selective detection of H_2O and D_2O by (2+1)-resonance enhanced multiphoton ionization, *J. Chem. Phys*., vol. 85, 6914-6922

Miles, R., Cohen, C., Conners, J., Howard, P., Huang, S., Markovitz, E., and Russell, G. (1987) Velocity measurements by vibrational tagging and fluorescent probing of oxygen, *Optics Letters*, vol. 12, no. 11, 861-863.

Miles, R. B., Connors, J. J., Markovitz, E. C., Howard, P. J., and Roth, G. J. (1989a) Instantaneous profiles and turbulence statistics of supersonic free shear layers by Raman Excitation plus Laser-Induced Electronic Fluorescence (RELIEF) velocity tagging of oxygen, *Exp. Fluids*, vol. 8, 17-24.

Miles, R. B., Connors, J. Markovitz, E., Howard, P., and Roth, G. (1989b) Instantaneous supersonic velocity profiles in an underexpanded sonic air jet by oxygen flow tagging, *Phys. Fluids A*, vol. 1, no.2, 389-393.

Miles, R. B., Zhou, D., Zhang, B., Lempert, W. R., and She, Z. S. (1993) Fundamental turbulence measurements by RELIEF flow tagging, *AIAA J*., vol. 31, no. 3, 447-452.

Miles, R. B. and Lempert, W. R. (1997) Quantitative flow visualization in unseeded flows, *Ann. Rev. Fluid Mech*., vol. 29, 285-326.

Miles, R. B., Grinstead, J., Kohl, R. H. and Diskin, G. (2000) The RELIEF flow tagging technique and its application in engine testing facilities and for helium-air mixing studies, *Meas. Sci. Technol*., vol. 11, no. 2, 1272-1281.

Miller, S. (1962) Photochemical reaction for the study of velocity patterns and profiles, B.A.Sc. thesis, University of Toronto, Ontario, Canada.

Mortellaro, M. A. and Nocera, D. G. (1996a) A turn-on for optical sensing, *Chem.Tech.*, vol.26, 17-23

Mortellaro, M. A. and Nocera, D. G. (1996b) A supramolecular chemosensor for aromatic hydrocarbons, *J. Am. Chem. Soc*., vol. 118, 7414-7415.

Mosier. B. P., Molho, J. I., and Santiago, J. G. (2002) Photobleached-fluorescence imaging of microflows, *Exp. Fluids*, vol. 33, 545–554.

Nocera, D. G. (1996) Not just another pretty shape, *New Scientist*, vol. 149, 24-27

Noullez, A., Wallace, G., Lempert, W, Miles, R. B., and Frisch, U. (1997) Transverse velocity increments in turbulent flow using the RELIEF technique, *J. Fluid Mech*., vol. 339, 287-307.

Ojha, M., Cobbold, R. S. C., Johnston, K. W., and Hummel, R. (1989) Pulsatile flow through constricted tubes: an experimental investigation using photochromic tracer methods, *J. Fluid Mech.*, vol. 203, 173-197.

Orlemann C., Schulz, C., and Wolfrum, J. (1999) NO-flow tagging by photodissociation of NO_2. A new approach for measuring small-scale flow structures, *Chem Phys Lett.* vol.307, no. 1-2, 15-20

Park, H., Moore, J. A., Trass, O. and Ojha, M. (1999) Laser photochromic velocimetry estimation of the vorticity and pressure field – two-dimensional flow in a curved vessel, *Exp Fluids*, vol.26, 55-62.

Park, J. S., Kim, H. J., and Kihm, K. D. (2001) Molecular tagging fluorescence velocimetry (MTFV) for Lagrangian flow field mapping inside evaporating meniscus: potential use for micro-scale applications, *J. Flow Visualization & Image Processing*, vol. 8, 177-187.

Paul, P. H., Garguilo, M. G., and Rakestraw, D. J. (1998) Imaging of pressure and electrokinetically driven flows through open capillaries, *Anal. Chem*., vol. 70, 2459-2467.

Pikramenou, Z., Yu J-A., Lessard, R. B., Ponce, A., Wong, P. A., and Nocera, D. G. (1994) Luminescence from supramolecules triggered by the molecular recognition of substrates, *Coord Chem Rev*., vol. 132, 181-194.

Pitz, R. W., Brown, T. M., Nandula, S. P., Skaggs, P. A., DeBarber, P. A., Brown, M. S., and Segall, J. (1996) Unseeded velocity measurement by ozone tagging velocimetry, *Optics Letters*, vol. 21, no. 10, 755-757.

Pitz, R. W., Wehrmeyer, J. A., Ribarov, L. A., Oguss, D. A., Batliwala, F., DeBarber, P. A., Deusch, S., and Dimotakis, P. E. (2000) Unseeded molecular flow tagging in cold and hot flows using ozone and hydroxyl tagging velocimetry, *Meas. Sci. Technol*., vol.11, no. 9, 1259-1271.

Pitz, R. W., Lahr, M. D., Douglas, Z. W., Wehrmeyer, J. A., Hu, S., Carter, C. D., Hsu, K.-Y., Lum, C., and Koochesfahani, M. M. (2005) "Hydroxyl tagging velocimetry in a supersonic flow over a cavity," *Applied Optics*, vol. 44, no. 31, 6692-6700.

Ponce, A., Wong, P. A., Way, J. J. and Nocera, D. G. (1993) Intense phosphorescence triggered by alcohols upon formation of a cyclodextrin ternary complex, *J. Physical Chem*., vol. 97, 11137-11142.

Popovich, A. T. and Hummel, R. L. (1967) A new method for non-disturbing turbulent flow measurement very close to a wall, *Chem. Eng. Soc.,* vol. 22, 21-25.

Rička, J. (1987) Photobleaching velocimetry, *Exp. Fluids*, vol. 5, 381-384.

Ribarov, L. A., Wehrmeyer, J. A., Batliwala, F., Pitz, R. W., and DeBarber, P. A. (1999) Ozone tagging velocimetry using narrowband excimer lasers, *AIAA J*., vol. 37, no. 6, 708-714.

Ribarov, L. A., Wehrmeyer, J. A., Pitz, R. W., and Yetter, R. A. (2002) Hydroxyl tagging velocimetry (HTV) in experimental airflows, *App. Phys. B*, vol. 74, 175-183.

Ribarov, L. A., Wehrmeyer, J. A., Hu, S., and Pitz, R. W. (2004) Multiline hydroxyl tagging velocimetry measurements in reacting and nonreacting experimental flows, *Exp. Fluids*, vol. 37, 65-74.

Rubinsztein-Dunlop, H., Littleton, B., Barker, P., Ljungberg, P., and Malmsten, Y. (2001) Ionic strontium fluorescence as a method for flow tagging velocimetry, *Exp. Fluids*, vol. 30, 36-42.

Rudzinski, C. M. and Nocera, D. G. (2001) Buckets of light, In *Optical Sensors and Switches*, V. Ramamurthy and K. S. Schanze, K. S. (Eds.), vol. 7, 1-90.

Sadr, R. and Klewicki, J. C. (2003a) An experimental investigation of the near-field flow development in coaxial jets, *Phys. Fluids*, vol. 15, no. 5, 1233-1246.

Sadr, R. and Klewicki, J. C. (2003b) A spline-based technique for estimating flow velocities using two-camera multi-line MTV, *Exp. Fluids*, vol. 35, 257-261.

Sadr, R. and Klewicki, J. C. (2005) Flow field characteristics in the near field region of particle-laden coaxial jets, *Exp. Fluids*, vol. 39, 885-894.

Schrum, K. F., Lancaster, J. M., Johnston, S. E, and Gilman, S. D. (2000) Monitoring electroosmotic flow by periodic photobleaching of a dilute, neutral fluorophore, *Anal. Chem*., vol. 72, 4317–4321.

Sijtsema, N. M., Dam, N. J., Klein-Douwel, R. J. H, and ter Meulen, J. J. (2002) Air photolysis and recombination tracking: A new molecular tagging velocimetry scheme, *AIAA J*., vol. 40, no. 6, 1061-1064.

Sinton, D., Xuan, X., and Li, D. (2004) Thermally induced velocity gradients in electroosmotic microchannel flows: the cooling influence of optical infrastructure, *Exp. Fluids*, vol. 37, 872-882.

Stier, B. and Koochesfahani, M. M. (1997) Molecular tagging velocimetry in gas phase and its application to jet flows, ASME Paper FEDSM97-3687.

Stier, B. and Koochesfahani, M. M. (1998) Whole field MTV measurements in a steady flow rig model on an IC engine, SAE Technical Paper 980481.

Stier, B. and Koochesfahani, M. M. (1999) Molecular tagging velocimetry (MTV) measurements in gas phase flows, *Exp. Fluids*, vol. 26, no. 4, 297-304.

Thomson, S. L. and Maynes, D. (2001) Spatially resolved temperature measurements in a liquid using laser induced phosphorescence, *J. Fluids Engr*., vol. 123, 293-302.

Thurlow, E. M. and Klewicki, J. C. (2000) Experimental study of turbulent Poiseuille–Couette flow, *Phys. Fluids*, vol. 12, no. 4, 865-875.

Tokumaru, P. T. and Dimotakis, P. E. (1995) Image correlation velocimetry, *Exp. Fluids*, vol. 19, pp. 1-15.

Turro, N.J. (1978) Modern Molecular Photochemistry, Menlo Park: Benjamin/Cummings

van der Laan, W. P. N., Tolboom, R. A. L., Dam, N.J., and ter Meulen, J. J. (2003) Molecular tagging velocimetry in the wake of an object in supersonic flow, *Exp. Fluids*, vol. 34, 531-533.

Wang, G. R. and Fiedler, H. E. (2000) On high spatial resolution scalar measurement with LIF. Part 1: Photobleaching and thermal blooming, *Exp Fluids*, vol. 29, 257-264.

Wang, G. R. (2005) Laser induced fluorescence photobleaching anemometer for microfluidic devices, *Lab Chip*, vol. 5, 450–456.

Wayne, R.P. (1980) Principles and Applications of Photochemistry. Oxford: Oxford University Press.

Wehrmeyer, J. A., Ribarov, L. A., Oguss, D. A., Batliwala, F., Pitz, R. W., and DeBarber, P. A. (1999a) Flow tagging velocimetry for low and high temperature flowfields, AIAA paper AIAA-99-0646.

Wehrmeyer, J. A., Ribarov, L. A., Oguss, D. A., and Pitz, R. W. (1999b) Flame flow tagging velocimetry with 193 nm H_2O photodissociation, *Applied Optics*, vol. 38, 6912-6917.

Wenz, G. (1994) Cyclodextrins as building blocks for supramolecular structures and functional units, *Angew. Chem. Int. Ed. Engl*., vol. 33, 803-822.

Wirtz, K., Koochesfahani, M. M., McGrath, J. J., and Benard, A. (1998) Molecular tagging velocimetry applied to buoyancy-driven convective phenomena during solidification, ASME Paper HTD-vol. 361-4, 103.

Yu, J-A., Lessard, R. B., and Nocera, D.G. (1991) Direct observation of intramolecular energy transfer from a β-diketonate to terbium(III) ion encapsulated in a cryptand, *Chem. Phys. Lett.*, vol. 187,263-268,

Yurechko, V.N. and Ryazantsev, Y. S. (1991) Fluid motion investigation by photochromic flow visualization technique, *Exp. Thermal Fluid Sci*., vol. 4, 273-288.

Zalzal, P., Ojha, M., Ethier, C. R., Cobbold, R. S. C. and Johnston, K. W. (1994) Visualization of transitional pipe flow using photochromic tracer method, *Phys Fluids*, vol. 6, 2003-2010.

Zheng, Q. and Klewicki, J. C. (2000) A fast data reduction algorithm for molecular tagging velocimetry: the decoupled spatial correlation technique, *Meas. Sci. Technol*., vol.11, no. 9, 1282-1288.